DOES ULTRASOUND STIMULATION IMPROVE THE QUALITY OR QUANTITY OF COLLAGEN IN ENGINEERED CARTILAGE?

A Thesis
Submitted to
The Temple University Graduate Board

In Partial Fulfillment
of the Requirements for the Degree
MASTER OF SCIENCE IN BIOENGINEERING

---

by
Michael J. Shockley
May 2013

Thesis Approvals:

Nancy Pleshko, Thesis Advisor, Department of Bioengineering
Won Hyuk Suh, Department of Bioengineering
Vanessa Yingling, Department of Kinesiology

Abstract

Articular cartilage is a highly specialized connective tissue in the body responsible for protecting and cushioning bony ends in diarthrodial joints. Despite the unique ability of this tough, spongy matrix to absorb repetitive stress and loading, cartilage damage is a common occurrence, and as cartilage possesses poor self-repair capabilities, tissue-engineered cartilage replacement is under development as a viable method of repair. Tissue-engineered constructs have thus far been unable to replicate the matrix composition of native cartilage satisfactorily enough to produce usable mechanical properties; in particular, collagen content is very low. One means of improving engineered construct composition may be pulsed low-intensity ultrasound (PLIUS), which is used clinically to stimulate healing of chronic bone lesions, and has been shown to affect chondrocytes in cartilage explants and engineered constructs. We believe it may be of use specifically in improving collagen quantity and quality in engineered constructs. FT-IR spectroscopy shows promise as a valuable tool in collagen crosslink maturity analysis, replacing the current expensive, complicated standard of HPLC and allowing for high-resolution spatial mapping of components. A spectral parameter has been established in literature as being related to collagen maturity in bone, which we explore as a potential means of assessing collagen quality in our engineered cartilage. The specific aims of this research are twofold: first, to assess whether PLIUS improves primary bovine chondrocyte-seeded poly-glycolic acid (PGA) mesh scaffold composition by culturing groups with and without PLIUS stimulation, and second, to correlate FT-IR parameters (including the aforementioned maturity parameter) from engineered cartilage specimens and pure crosslink peptides to mechanical testing in unconfined compression.

Acknowledgement

I am grateful to have such a strong, widespread support system, all of whom share in some part the responsibility for this work. In particular, I would like to thank my advisor, Dr. Nancy Pleshko, for a number of reasons, from her constant support and insight into the project to her ability to stress over its results and deadlines and not show it. I would like to thank all of the members of the Temple University Tissue Imaging & Spectroscopy Lab with whom I have had the pleasure of working, and who tirelessly trudged through the trenches alongside me in the advancement of this project and others. In particular I would like to thank TISL's Postdoctoral Fellow, Cushla McGoverin, for the input and knowledge she constantly gave, and for her many tireless roles in the lab, some spectroscopic, others far from. Arash Hanifi, a previous TISL member, also deserves recognition, as his work provided the seed for this project. I would like to thank Drs. Won Suh and Vanessa Yingling for agreeing to serve on my thesis committee, Drs. Alan Grodzinsky and Eliot Frank from the Massachusetts Institute of Technology for the mechanical testing of our tissue engineered cartilage constructs, and Drs. Mitsuo Yamauchi and Masahiko Terajima from the University of North Carolina for the isolation and purification of crosslink peptides. Finally, I would like to thank my family and friends for their support throughout my time at Temple University.

Dedication

To my parents, Michael and Lori,

and my siblings Matt and Steph,

for adding color and comic relief

to a typically greyscale and dramatic world.

TABLE OF CONTENTS

List of Figures

List of Tables

CHAPTER 1

INTRODUCTION

Cartilage

Cartilage is a set of highly specialized protective and connecting tissues comprised of three general types: hyaline cartilage, fibrocartilage and elastic cartilage. It varies in composition by type, specific anatomical location and physiological application [1]. Articular cartilage is a form of hyaline cartilage lining the articulating surfaces of bones in diarthrodial joints such as the knee, and is responsible for cushioning and protecting the surfaces from the high stress levels imposed upon the joints. Chondrocytes are the only cell type present, and are responsible for replacement of degraded matrix molecules for proper maintenance of the tissue during wear [1]. Because of the unique stresses imposed upon cartilage, it is hypocellular, avascular, aneural and alymphatic. The nutrition of articular cartilage as a result is derived almost entirely from the synovial fluid in the joint capsule, which is circulated throughout the extracellular matrix as the

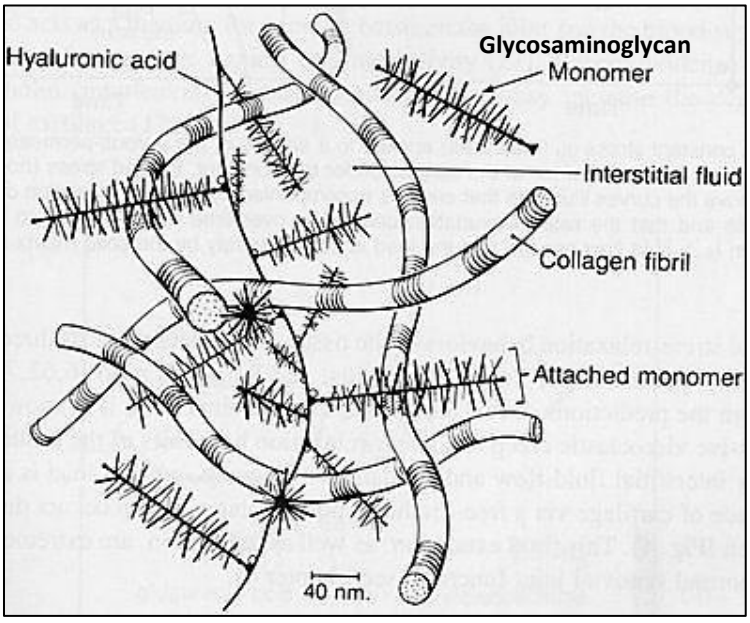

Figure 1. Cartilage extracellular matrix components. (Adapted from [2])

cartilage is mechanically loaded and unloaded through daily use in a fashion analogous to squeezing and refilling a sponge.

Cartilage is primarily comprised of collagen (15-25% by wet weight), mainly type II in articular cartilage, proteoglycans (5-10%), chondrocytes (5%), and water (70-80%) [2]. Collagen lends tensile strength to the cartilage, while proteoglycans bind water and together are responsible for the bulk of compressive strength. Articular cartilage is organized in a highly zonal structure, shown in Fig. 2. The superficial tangential zone nearest the articulating surface contains a high volume of collagen fibrils, primarily oriented parallel with the surface, believed to aid in resisting shear forces [3]. Chondrocytes in the superficial zone are elongated parallel to the surface as well, and the highest volume of water and lowest volume of proteoglycans exist there. Collagen fibrils and chondrocytes are oriented randomly throughout the middle zone. In the deep zone, near the bone, collagen fibrils are perpendicularly oriented to the surface, believed to contribute to anchorage of the cartilage to the bone and resistance to delamination [4]. Chondrocytes in the deep zone aggregate in columnar lines, and the deep zone contains the highest volume of proteoglycans.

Articular Cartilage Mechanics

The main purpose of cartilage is to maintain structural integrity of the joints, absorb compressive stress, resist shear forces by acting together with synovial fluid as a joint lubricating system, and protect the underlying bone. Mechanically, cartilage is considered to be a biphasic material comprised of a solid matrix phase and a fluid water phase [4]. This lends it viscoelastic properties, as the relationship between applied load and resultant deformation is rate-dependent. Cartilage exhibits stress relaxation when

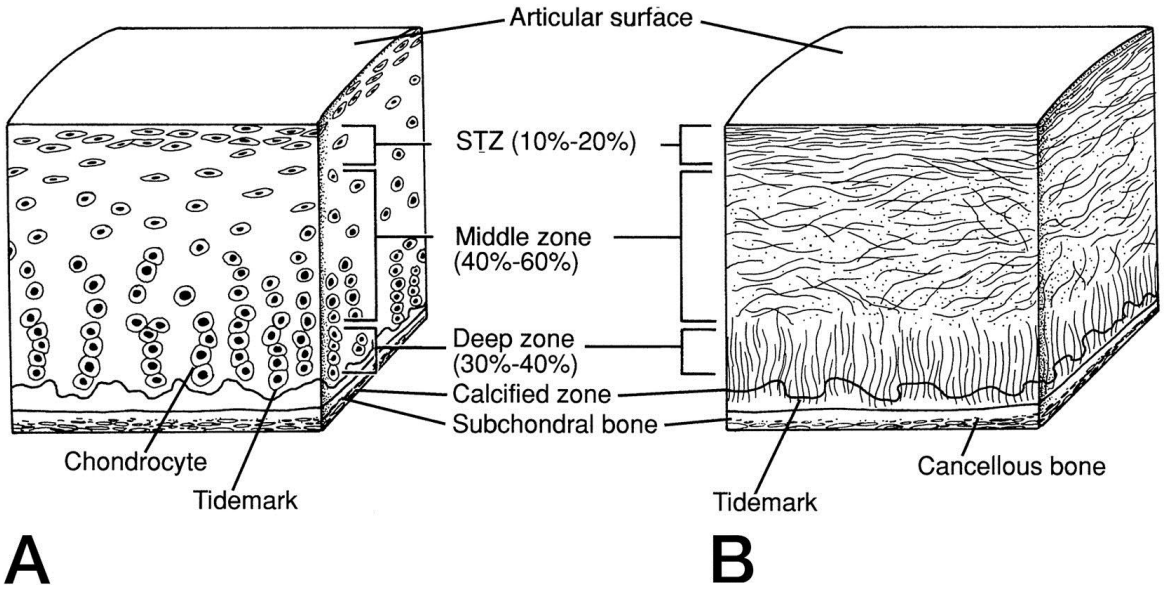

Figure 2. Zonal organization of articular cartilage with respect to (a) cells and (b) collagen fibers. (Adapted from [4])

deformed: upon compression, the fluid phase flows out of the matrix, decreasing the apparent stress, as seen in Fig. 3. The greater the deformation rate, the stiffer cartilage becomes to compensate. This is critical to long-term mechanical integrity, as impacts which deform cartilage quickly are generally higher energy impacts, and stiffening increases the shock energy which cartilage is able to absorb and shield from bone. Articular cartilage can withstand compressive strains up to roughly 60%, but typical physiological loading of the knee does not exceed 15% compressive strain. Dynamically, typical physiological loading occurs within the frequency range of 0.1-2 Hz [5].

Articular cartilage is mechanically tested in compression in a number of ways. In general, three overall paradigms exist: unconfined compression, in which cartilage is loaded in solution between two flat nonporous platens, and interstitial fluid is allowed to flow freely through the sides; confined compression, in which the cartilage is restricted on all sides and unable to perfuse interstitial fluid out, and is compressed by a porous platen through which fluid flow occurs; and indentation testing, in which a small indenter

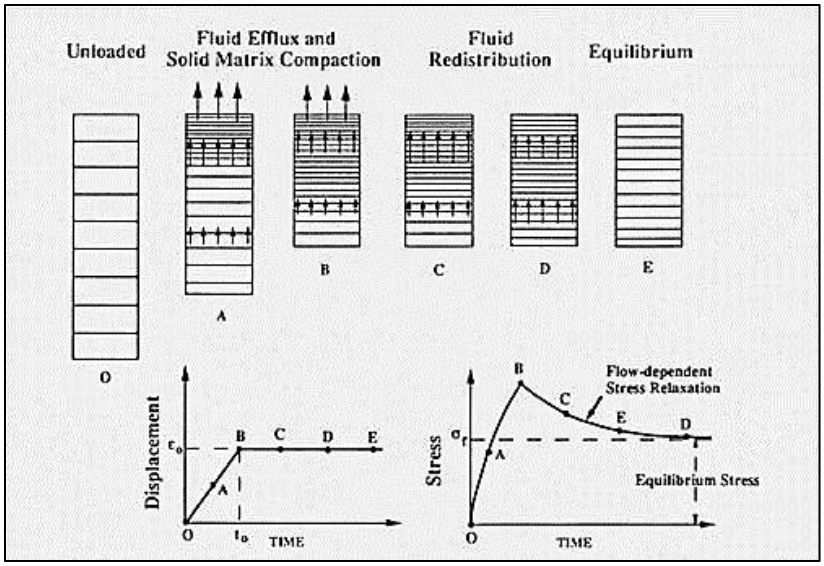

Figure 3. Mechanics of articular cartilage, showing stress relaxation and fluid redistribution upon compressive loading. (Adapted from [6])

(ranging from fractions of millimeters to fractions of micrometers in diameter) is used to test the surface [6]. All have their advantages; we chose to use unconfined compression, as it is arguably most commonly used in literature and provides several important mechanical parameters, notably equilibrium stiffness and dynamic stiffness.

Equilibrium stiffness is defined as the slope of stress-strain data points taken from cartilage at steady-state fluid flow, i.e. as the cartilage has reached equilibrium and net fluid flow is zero [7]. It is analogous to the Young's modulus of classical mechanics, and can be seen as a measure of the ability of the cartilage matrix to resist compression when fluid flow is not a factor—in effect, it measures the elastic response of a viscoelastic material [5]. Dynamic stiffness, on the other hand, is defined as the change in output stress over the change in input strain as a specimen is sinusoidally loaded [8]. It is a measure of the instantaneous response of cartilage to mechanical insult [9]. Due to the rate dependence of cartilage mechanics, dynamic stiffness is typically computed over a

range of physiologically relevant oscillatory loading frequencies, and increases with increasing loading frequency [8].

Cartilage Damage and Repair

Despite the unique ability of cartilage to absorb repetitive mechanical stress and loading, cartilage injury is a common occurrence. It was estimated in 2005 that over 600,000 procedures per year take place to repair articular cartilage; that number has undoubtedly grown since [10]. The two most common modes of articular cartilage damage are acute injuries sustained during sports and accidents and osteoarthritis, a degenerative disease causing the cartilage to wear away. Cartilage does not repair well, with neither the immune cells nor vasculature necessary to provoke an inflammatory response, and due to its hypocellular nature, repair by native chondrocytes is slow, and repair cartilage displays poor mechanical properties compared to surrounding healthy tissue [1]. There are a number of clinical interventions currently employed to repair damaged cartilage [11, 12]. Surgeons may arthroscopically debride the damaged area, removing fibrillations and smoothing the articular surface. This provides good short-term results, though the mechanical integrity is compromised and leads to softer tissue. Microfracture involves the removal of damaged cartilage and debridement of the subchondral bone, causing bleeding; the wound site fills with blood and forms a fibrin plug, allowing mesenchymal stem cells to migrate into the area and create new cartilage. Unfortunately, repair (scar) cartilage is primarily fibrocartilage, and displays poor mechanical properties compared to surrounding healthy cartilage. Grafts may be taken from either the patient or an external source and implanted into the wound site, though it is a highly technical procedure and complications arising from improper fusion of the

grafts to surrounding healthy tissue are common. Finally, surgeons may perform an autologous chondrocyte implantation, wherein cartilage is harvested from a less-loaded area of the joint, chondrocytes are extracted and expanded in culture, a flap of periosteum is sewn over the wound site, and the cells are injected into the site and allowed to grow new cartilage. This procedure compares favorably in most studies to grafting, but resultant tissue is softer than—and therefore inferior to—native cartilage [13].

Tissue Engineering and Pulsed Low-Intensity Ultrasound (PLIUS) Stimulation

One of the most promising repair techniques under research and development is tissue engineering cartilage constructs [14]. In short, chondrocytes are harvested from a less-loaded area of the joint as in autologous chondrocyte implantation and expanded in culture. They are seeded into three-dimensional bioresorbable scaffolds and cultured under standard sterile cell culture conditions as the chondrocytes adhere, proliferate, and deposit new matrix. Once the construct is established, it is implanted into the wound site to replace the damaged cartilage. Over time, the scaffold material degrades and is resorbed back into the body, leaving behind healthy engineered cartilage. The process is shown in Fig. 4.

Despite much interest in the area and substantial resources expended to this end, the technology is not yet at a level which produces viable replacement cartilage. Constructs inevitably display suboptimal matrix composition, low in collagen and containing variable quantities of proteoglycans and chondrocytes [15]. This leads to mechanically inferior tissue [7]. One means of increasing the mechanical properties of engineered cartilage may be stimulation via pulsed low-intensity ultrasound (PLIUS). PLIUS was originally shown to increase bone matrix deposition and improve mechanical

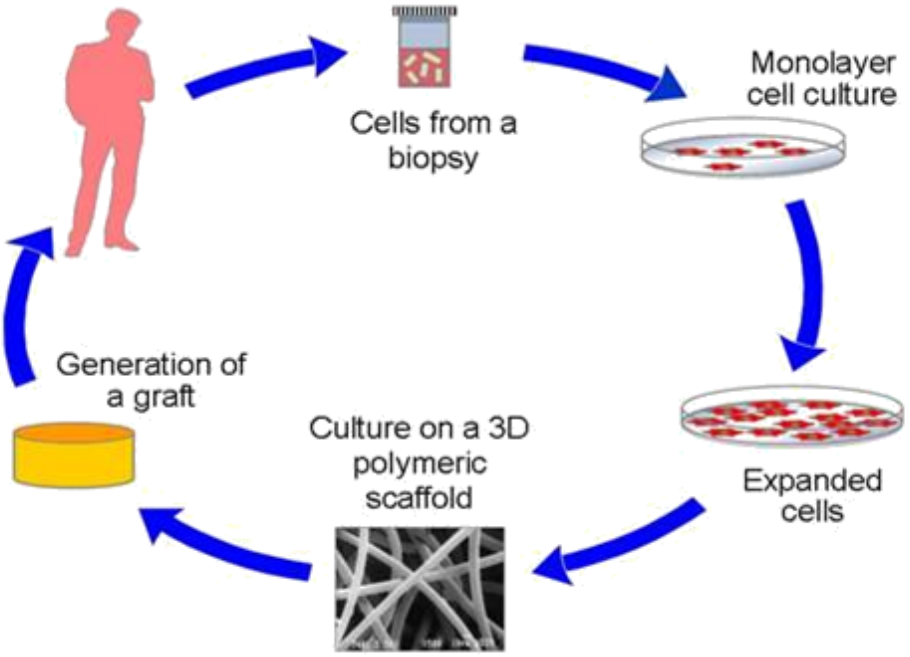

Figure 4. Tissue engineering to replace damaged tissue. (Adapted from [16])

properties; it is currently in clinical use as a means to stimulate fracture healing in chronic bone lesions and nonunions in cases where surgery fails to remedy the issue [17, 18]. The first therapeutic PLIUS device approved by the FDA for clinical use was the Exogen Bone Healing System (Smith & Nephew Inc, Memphis, TN), and as such most PLIUS devices use the same loading paradigm. Patients are provided an ultrasound transducer with a set loading cycle (1.5 MHz sine wave ultrasound pulse with an intensity of 30 mW/cm^2 repeated at 1 kHz with a duty cycle of 20%) and instructed to use it for a preset 20 minutes per day, coupled directly to the skin via ultrasound gel [19]. Cartilage has been shown to respond to PLIUS as well [20, 21]. While it has been known for years that cartilage responds to mechanical loading by increasing its matrix and mechanical properties [22], recent work by Perry et al. implied that PLIUS acts on chondrocytes by mimicking normal physiological loading [23]. These findings are debatable, however, given work by Takeuchi et al. which found that PLIUS stimulated cell signaling

pathways associated more with proliferation than response to more traditional cyclic mechanical loading [24-26]. It was briefly thought to be a possibility that a heating effect of the ultrasound transducer was causing the benefits, but a study by Chang et al. showed that the heating effect of clinical ultrasound transducers is insignificant, and work by Weidman and Tavakkoli implied that the increase is due to some reason other than heating [19, 27]. So there is still much work to be performed in order to gain a more complete understanding of the effects of ultrasound on chondrocytes. One recent double-blind, randomized, placebo-controlled pilot study published by Loyola-Sánchez et al. found that PLIUS stimulation of osteoarthritic knees improved medial tibial cartilage thickness in some patients, and suggested that the effect be subject to further clinical research [28]. In addition, several groups have published findings in support of ultrasound stimulation of engineered cartilage specifically [29-31]. With these findings there seems to be reason to believe that ultrasound will significantly improve engineered constructs' composition.

Collagen Crosslinking

One important determinant of tissue quality is the crosslinking of collagen fibrils in cartilage. Collagen is highly crosslinked for mechanical integrity of the matrix [32, 33]. Typically the C-terminus end of one collagen fibril forms a crosslink with the N-terminus end of another [34]. This is an enzymatic reaction mediated by lysyl oxidase between lysyl and hydroxylysyl residues [35]. Immature crosslinks are composed of dihydroxylysinorleucine (DHLNL) and form divalent bonds connecting the two collagen fibrils, while mature crosslinks are pyridinoline and form trivalent bonds connecting three fibrils [32, 33]. Both are shown in Fig. 5. As mammals mature, the quantity of immature

crosslinks decreases and the quantity of mature crosslinks increases [36]. The maturation of these collagen crosslinks is extremely important for the mechanical stability of cartilage. Mechanical properties of cartilage increase with age and cross-linking maturity [37]. Bastiaansen-Jenniskens et al. showed that crosslinking inhibition in engineered cartilage constructs prevents their compressive mechanical properties from improving, and removing inhibitors allowed crosslinks to form again and compressive mechanical properties increased accordingly [38]. Since it affects compressive mechanical parameters so markedly, collagen crosslinking may be an important factor to analyze further. The effects of PLIUS on collagen crosslinking have not yet been the subject of peer-reviewed research.

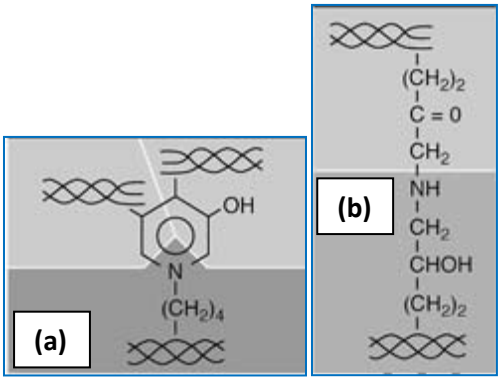

Figure 5. Collagen crosslinks: (a) mature pyridinoline, (b) immature DHLNL. (Adapted from [32])

Fourier Transform Infrared (FT-IR) Spectroscopy

The current standard method for analysis of pyridinoline and DHLNL is high performance liquid chromatography (HPLC) followed by mass spectrometry [39]. However, due to its cost and complexity, an alternative method of crosslink analysis would be welcome. Fourier Transform Infrared (FT-IR) spectroscopy is a method of compositional analysis based on interaction of infrared beams with molecular bonds in a

sample. Molecules are associated with a unique IR spectrum due to the molecular vibrations caused by the beam based on the molecule's structure and the frequency of IR radiation absorbed by it. When coupled with a microscopic stage and an array detector, an IR beam may be rastered across a specimen, collecting a unique spectrum at each point, forming a hyperspectral image of the specimen with a spatial resolution on the order of microns. This allows high-resolution compositional mapping across the specimen.

Of the three ranges of IR radiation (near-, mid- and far-IR), the mid-IR range of the cartilage spectrum has been the most well characterized thus far [40]. A representative cartilage mid-IR spectrum is shown in Fig. 6 with its bands and their associated vibrational modes labeled. The amide bands and side chain bands are associated with bond vibrations in protein structure, the majority of which in articular cartilage is type II collagen. The amide I band centered at 1655 cm^{-1} is caused mostly by C=O stretch of proteins, with some small contribution from proteoglycans [41]. The small band centered at 1338 cm^{-1} has been linked to the CH_2 side chains of the collagen helix, and when normalized with respect to the amide II band at 1550 cm^{-1} provides a measure of collagen integrity. Smaller peaks due to proteoglycans also exist, the most commonly studied one being centered at 850 cm^{-1} and caused by C-O-S stretch. Although infrared absorbance bands in cartilage have been associated with collagen and proteoglycan molecules, collagen crosslinks in cartilage have not been evaluated by FT-IR spectroscopy to date. However, FT-IR has been used to analyze collagen crosslinks in bone [36, 40, 42-44], where it was proposed that sub-bands centered at 1660 and 1690

cm^{-1} resolved from within the amide I peak could be related to pyridinoline and DHLNL, respectively [42]. The sub-peak bands were originally distinguished through the use of

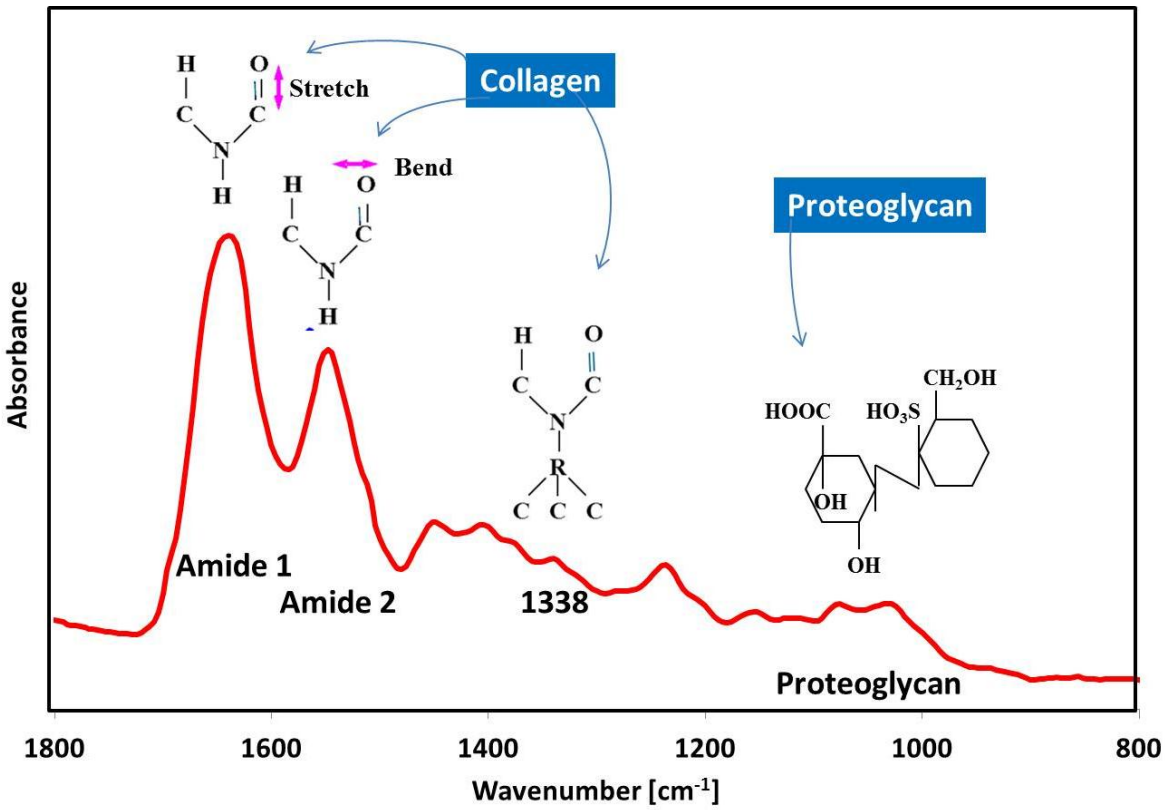

Figure 6. Typical mid-infrared spectrum of cartilage with peaks and corresponding vibrational modes.

second derivative spectroscopy, which allows for enhanced resolution of spectral features including the sub-band peaks centered at 1660 and 1690 cm^{-1}. The authors proposed that the 1660 cm^{-1} peak corresponded directly to pyridinoline and 1690 cm^{-1} directly to DHLNL, and a ratio of the 1660/1690 cm^{-1} peak areas could be taken as a measure of the ratio of pyridinoline/DHLNL in a sample. More recent research has used the ratio of the peak intensities at 1660 and 1690 cm^{-1}, which has the benefit of being more straightforward and robust due to the inherently high levels of subjectivity and user variability involved with curve-fitting [45]. However, Farlay et al. recently published data

implying that the 1660/1690 cm^{-1} ratio was independent of the levels of mature and immature crosslinks, but that it did increase with age, and proposed that the parameter be interpreted as a more general measure of collagen maturity [43]. While this has not yet satisfactorily been resolved, it seems logical that this parameter should be measured and may be a useful means of analyzing the maturity of the collagen in engineered constructs. In addition, the bulk of this research has been performed on collagen from bone, so the translation of the 1660/1690 cm^{-1} parameter to cartilage research would be beneficial as well.

CHAPTER 2

HYPOTHESES AND SPECIFIC AIMS

Hypothesis 1

PLIUS will increase the matrix deposition and therefore size of engineered cartilage constructs, resulting in increased bulk mechanical properties.

Aim 1

To assess improvement imparted by PLIUS to chondrocyte-seeded polyglycolic acid (PGA) mesh constructs by culturing these constructs with and without PLIUS stimulation for comparison. Geometrical and mechanical properties will be evaluated at each timepoint.

Hypothesis 2

FT-IR spectroscopy is a viable means of monitoring the collagen component of cartilage construct growth and maturation, due to changes in molecular bond vibrations.

Aim 2

To obtain FT-IR data from tissue engineered cartilage and correlate FT-IR parameters to mechanical data taken from tissue engineered cartilage specimens, as well as purified cartilage pyridinoline crosslink peptide samples, native cartilage, and cartilage samples with proteoglycans enzymatically digested and removed. Assessments of collagen properties will be made for PLIUS treatment and timepoint.

CHAPTER 3

TISSUE ENGINEERING AND PLIUS

Methods: Ultrasound validation

A clinically available pulsed low-intensity ultrasound (PLIUS) device (Exogen Bone Healing System, Smith & Nephew Inc., Memphis, TN) with six identical transducer heads was utilized for PLIUS application. Prior to use, preliminary tests were performed to ensure the proper power intensity output for the given experimental design using an Adventurer Pro radiation force balance (RFB) (Ohaus, Parsippany, NJ). Briefly, water was degassed via microwave for 30 minutes to eliminate cavitation effects of microbubbles, then the bottle was sealed and allowed to cool. The water was poured into the RFB, and the transducer was affixed in the RFB. The RFB was zeroed before and after the water was poured in, and after the transducer was placed just into the water. Care was taken to keep the ultrasonic wave path length the same with each test. The transducer was turned on and allowed to equilibrate for 60 s. The transducer was tested in four configurations, alone, coupled via gel to a polystyrene disc wider than the transducer and the same thickness as a well plate bottom, coupled to a glass coverslip 0.170 mm thick (the same thickness as the glass in the glass-bottom tissue culture plates used in this project), orcoupled to a detached well of a glass-bottom tissue culture plate. This was repeated n=6 times under each condition. The results are shown in Fig. 7, with measurements taken every 10 s for the first 60 s as the transducer equilibrated. It was found that of the expected average transducer intensity of 30 mW/cm^2, the transducer was recorded at an average of 22.0 mW/cm^2 with no covering and not significantly differently with a polystyrene layer (21.6 mW/cm^2, 98% of bare transducer output), but well lower with the coverslip glass (7.3 mW/cm^2, 33%). The tissue culture plate well, by

comparison, was measured at an average of 18.4 mW/cm^2, or 84% of bare transducer output. While substantially lower than the output of a bare transducer, the glass-bottom tissue culture dish was considered to transmit enough ultrasound to warrant its use. The presumed reason for this difference between glass-bottom culture dish and glass coverslip is that the glass in the center attenuated much of the ultrasound passing through it, but the bulk of the ultrasound waves are still able to transmit relatively undeterred through the plastic around it and into the media.

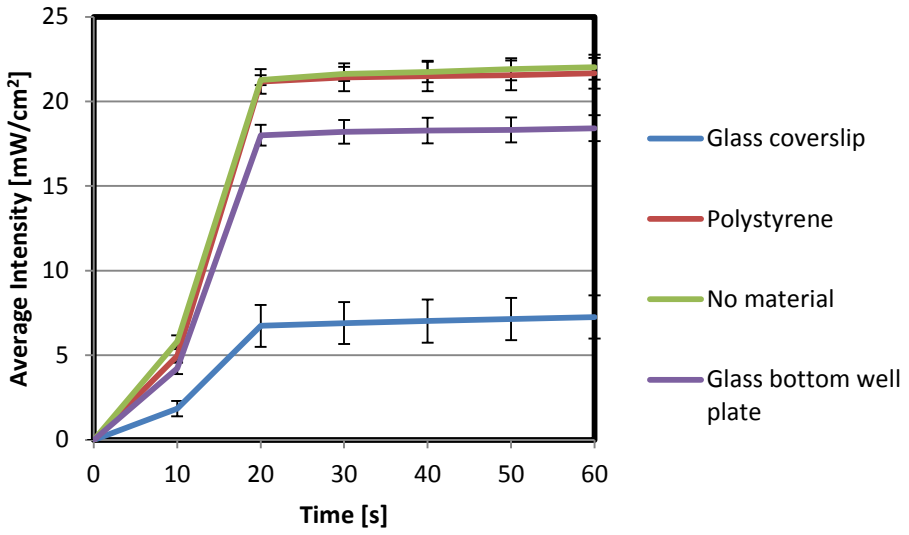

Figure 7. Comparison of ultrasound intensity output through different media.

Methods: Cell Harvest and Seeding

Cell harvest and seeding was performed according to a well-validated protocol [7, 15, 46, 47]. Fresh bovine stifle joints with synovial capsule intact were obtained from an FDA-approved slaughterhouse (Research 87, Boylston, MA) within 24 hours of slaughter. Articular cartilage was harvested aseptically from the femoral condyles and femoropatellar groove by gridding into 1 mm cubes and excision (Fig. 8a), followed by 3 consecutive PBS washes to remove traces of blood. Cartilage was digested for 12 hours

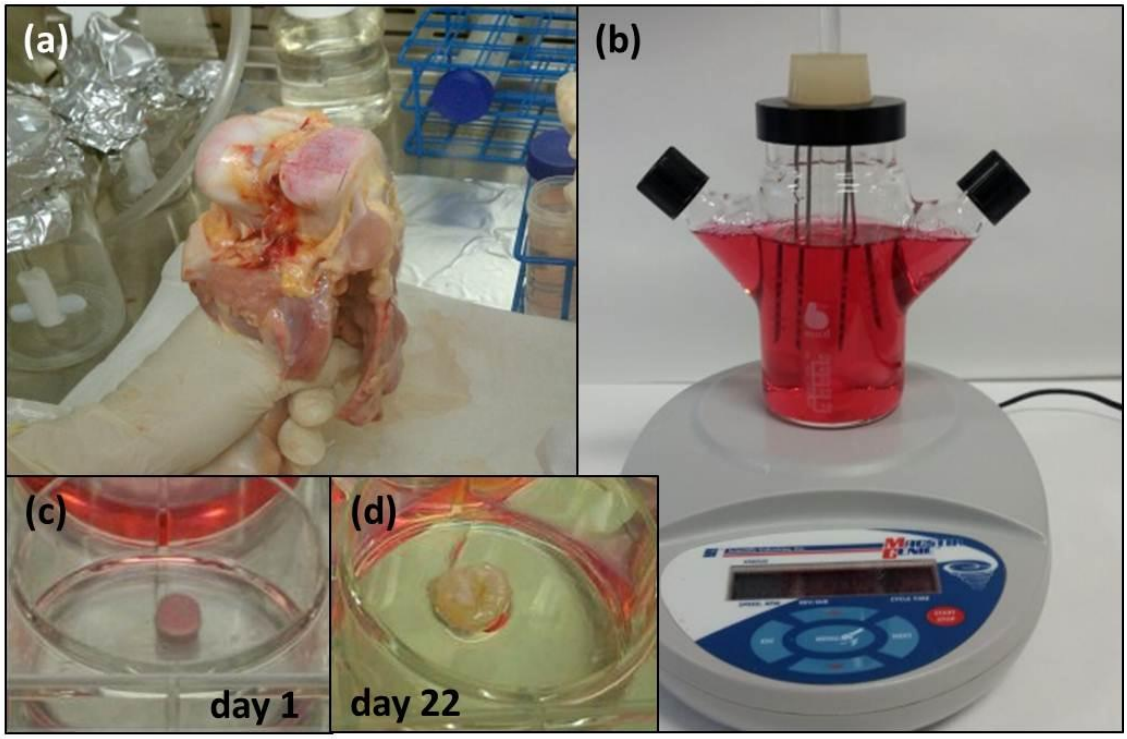

Figure 8. Macrophotograph of cell harvest and seeding. (a) Primary bovine chondrocytes were harvested from articular cartilage. (b) Chondrocytes were seeded onto PGA scaffolds suspended in spinner flasks. Scaffolds visibly grew in culture (c) from day 1 to (d) 3- and 5-week timepoints.

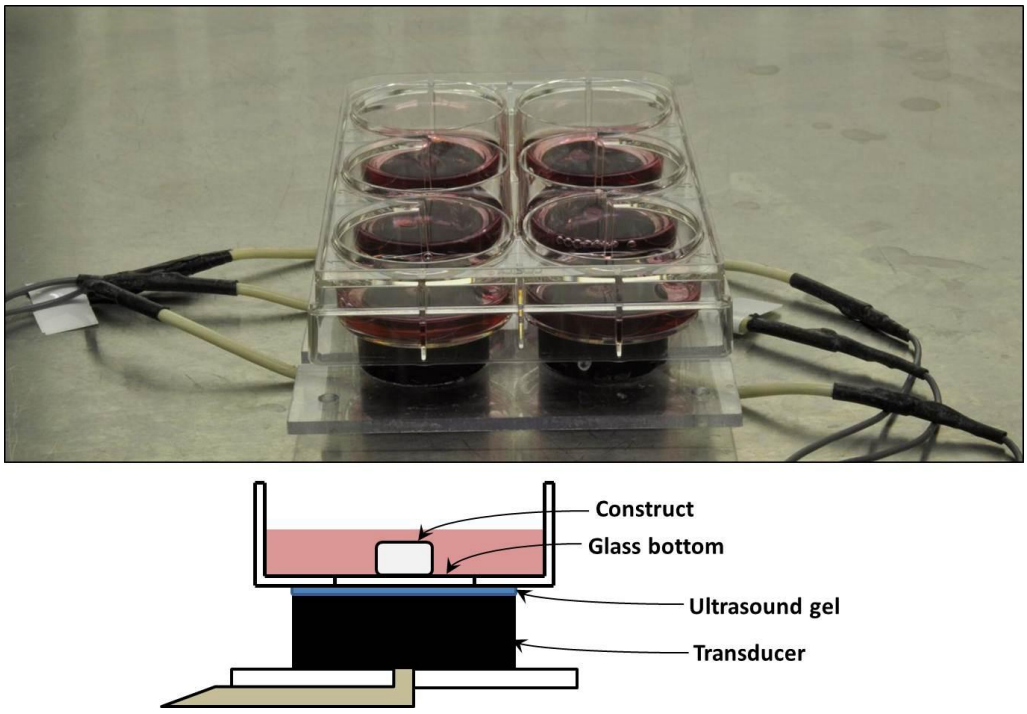

Figure 9. PLIUS treatment setup with side-view diagram.

in standard DMEM containing collagenase type II enzyme to free the chondrocytes from the surrounding matrix, in spinner flasks at ~80 RPM. This speed was fast enough to continually agitate the media while being shown in literature to be slow enough as to not damage suspended cells [7]. The resultant cell suspension was filtered out, centrifuged to pellet form, resuspended, and counted via trypan blue exclusion staining. The cells were then seeded at $2 \cdot 10^7$ cells per 5 mm scaffold for 72 hours in spinner flasks. Polyglycolic acid (PGA, Fig. 10) nonwoven mesh scaffolds were used because they are easy to handle, the material is well-studied in the biomedical context, has a high porosity amenable to cell infiltration and proliferation, has a degradation rate well suited for the cartilage growth timeline, and degrades through bulk hydrolysis into glycolic acid monomers, which are found naturally in the body and harmlessly enter the citric acid cycle [14]. The resultant constructs were cultured in six-well plates for 3 or 5 weeks under standard cell culture conditions, being treated with PLIUS for 20 minutes per day, 5 days per week using the aforementioned Exogen device, as shown in Fig. 9. An untreated control set was exposed to identical conditions, omitting PLIUS.

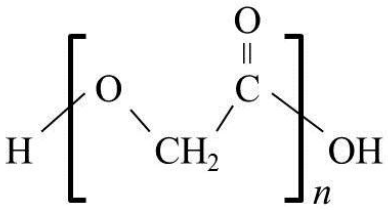

Figure 10. Molecular structure of polyglycolic acid (PGA).

Methods: Mechanical Testing

At the specified timepoints, typically after 3 and 5 weeks growth,constructs were harvested and tested under unconfined axial compression conditions, performed by collaborators from the Grodzinsky lab at the Massachusetts Institute of Technology

(Cambridge, MA). Specimen thicknesses were measured using a custom current-detecting micrometer which indicated when contact was made by the micrometer head and specimen [48]. The specimen was patted dry and weighed and the effective area calculated as weight (as estimate of volume) divided by height. The specimen was loaded axially between custom machined compression platens designed to keep the test specimens immersed in PBS with protease inhibitors during testing. Each specimen was loaded linearly to 5, 10, 12.5 and 15% strain consecutively, with a ramp time of 60 s for each then held for 600 s after each ramp to allow for stress relaxation/equilibration. Load was recorded at the quasi-equilibrium point at the end of the 10, 12.5 and 15% strain hold periods, and stress computed. Equilibrium stiffness was computed from the slope of the three points on a stress-strain plot. The specimens were then oscillated at 9 frequencies ranging from 0.005 to 2 Hz, and dynamic stiffness computed as dynamic (peak to peak) stress amplitude divided by dynamic (peak to peak) strain amplitude [49]. The loading curve is found in Fig. 11.

Methods: Statistical Analysis

All statistical analyses were performed using the SigmaPlot 12.0 software package (Systat Software Inc., San Jose, CA). Two-way analyses of variance (ANOVA) were performed to detect the effects of time in culture and ultrasound treatment on the mechanical properties of the constructs, with Holm-Sidak post-hoc testing, and significance between groups at the $p < 0.05$ level. A total of 6 experiments with $n = 33$ constructs per group were performed over the period of my thesis research. As not all these experiments were successful, the Results section includes data from $n = 3$ per treatment and timepoint.

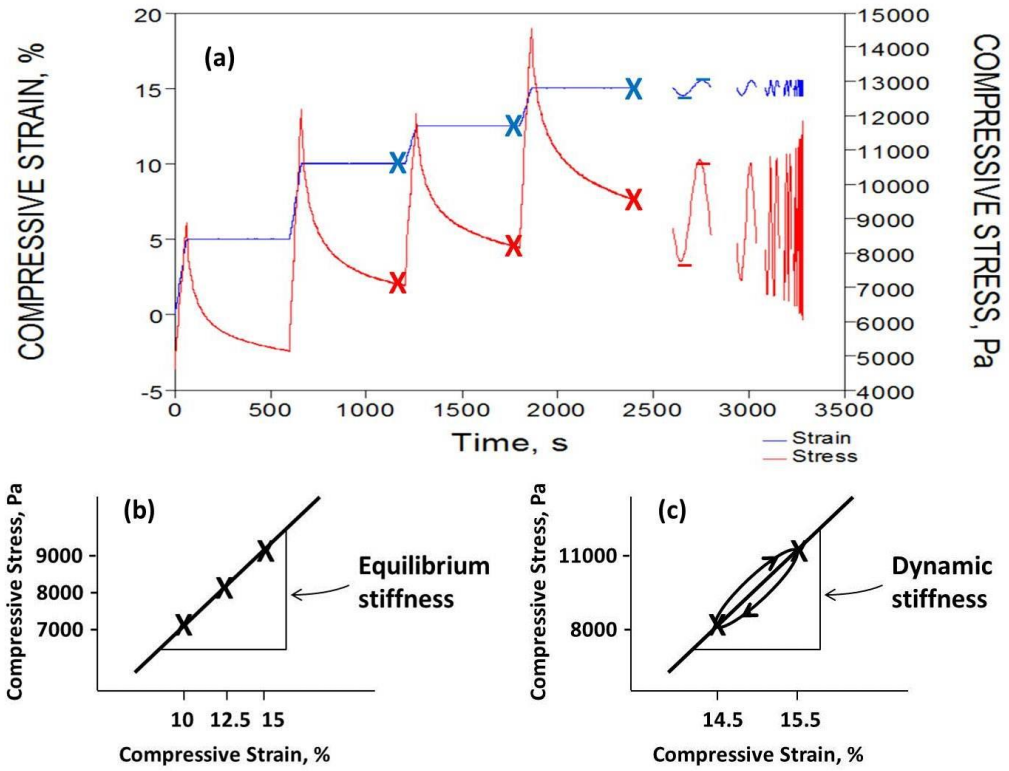

Figure 11. (a) Loading curve (blue) and corresponding stress output (red). Measurements for equilibrium stiffness were taken at each X on the stress and strain curves, and were used to compute equilibrium stiffness in (b). Measurements for dynamic stiffness were taken at each dash on the stress and strain curves, and were used as in (c).

Results

Growth of the tissue engineered cartilage constructs was substantial for the first three weeks, but afterwards stabilized. Construct wet weight, thickness, cross-sectional area, and volume measurements are shown in Fig. 12. Cross-sectional area increased significantly from 3 to 5 weeks overall and in the control group; increase was not significant in the ultrasound group.

Overall, the equilibrium stiffness was found to improve significantly with time, but not with treatment (Fig. 13). However, there were a number of statistical interactions within groups. Equilibrium stiffness was found to be significantly higher in the

ultrasound group at the 5-week timepoint but not at the 3-week timepoint. In addition, the equilibrium stiffness increased significantly over time in the ultrasound groups, but not with the control groups. Dynamic stiffness followed these same trends across all loading frequencies tested (Fig. 14).

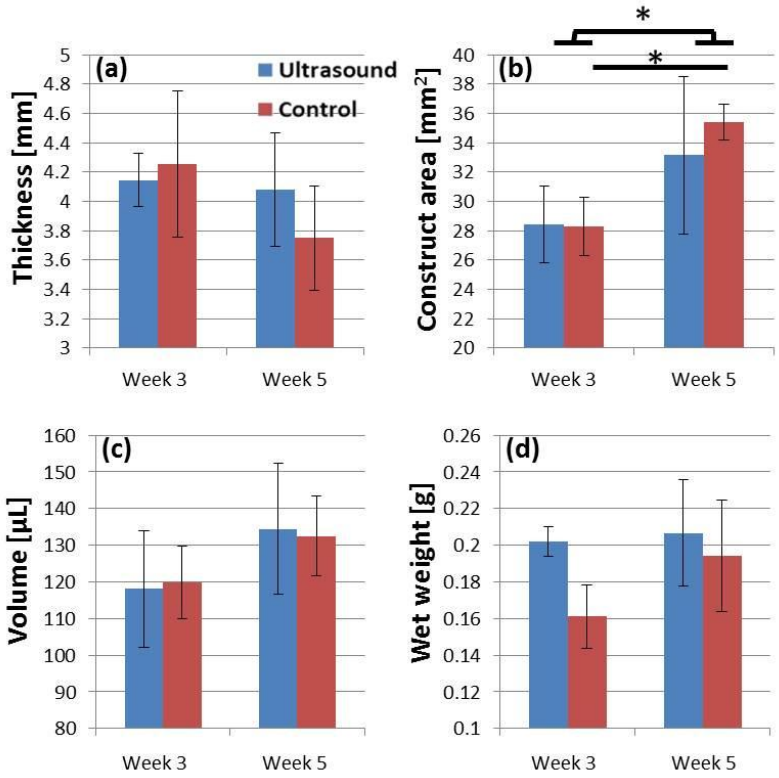

Figure 12. Geometrical construct data showing growth over time. (a) Thickness showed no significant difference between 3 and 5 week timepoints or between treatments; constructs were 2 mm thick at seeding. (b) Cross-sectional area increased significantly over time overall and within the control group; constructs had an initial area of 19.6 mm^2 at seeding. (c) Construct volume experienced a nonsignificant increase over time; constructs were 39.3 µL at seeding. (d) Wet weight showed no significant difference across treatment or timepoint groups; average wet weight at seeding was 0.035 g.

Discussion

The goal of this part of the study was to assess effects of pulsed low-intensity ultrasound treatment on the geometrical and mechanical properties of tissue engineered

cartilage constructs grown in culture over the course of several weeks. Mechanical integrity of the engineered cartilage was deemed the most important outcome, as the purpose of articular cartilage in the body is to withstand compressive stresses and protect the underlying bone, and tissue engineered cartilage would be required to fulfill the same function. Ultrasound was shown to improve the compressive strength of the cartilage as quanitifed by equilibrium and dynamic stiffnesses, but only at the 5-week timepoint. In addition, while mechanical stiffness was increased, the resultant constructs were still at least an order of magnitude weaker than that of native cartilage (25–40 kPa equilibrium stiffnesses compared to ~400 kPa in native cartilage, and 0.4-1.0 MPa dynamic stiffnesses at 1 Hz compared to ~16 MHz in native cartilage). These findings, while seemingly very low, match previous tissue engineered cartilage studies, in particular those grown on PGA scaffolds. The work pioneering this area, performed by Vunjak-Novakovic et al., reported equilibrium moduli of around 50 kPa and dynamic stiffnesses of around 1 MPa at 1 Hz after 6 weeks in culture, matching the mechanical parameters

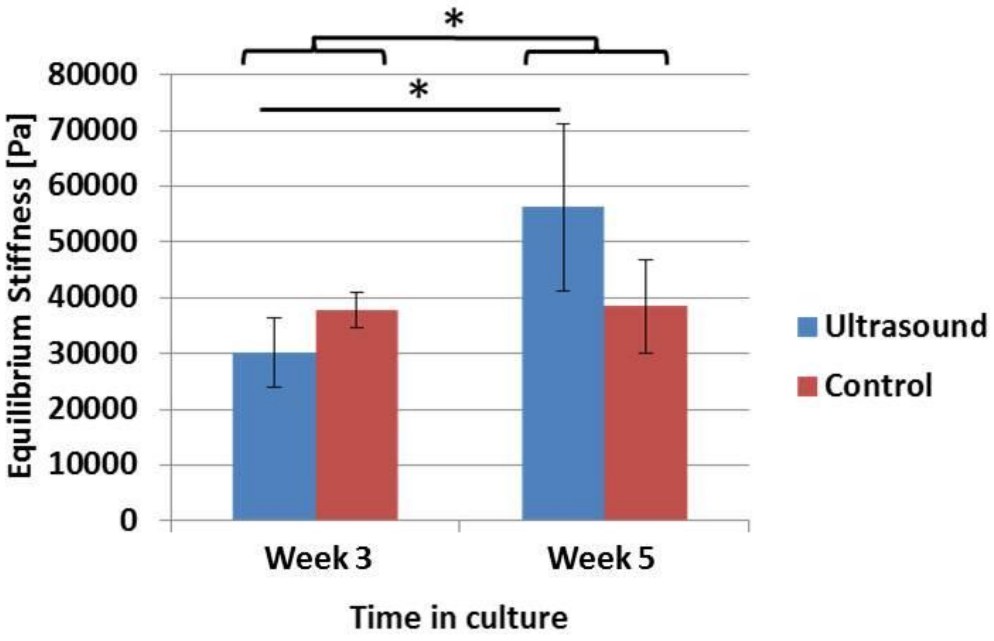

Figure 13. Equilibrium stiffness over time with respect to treatment. (* p < 0.05)

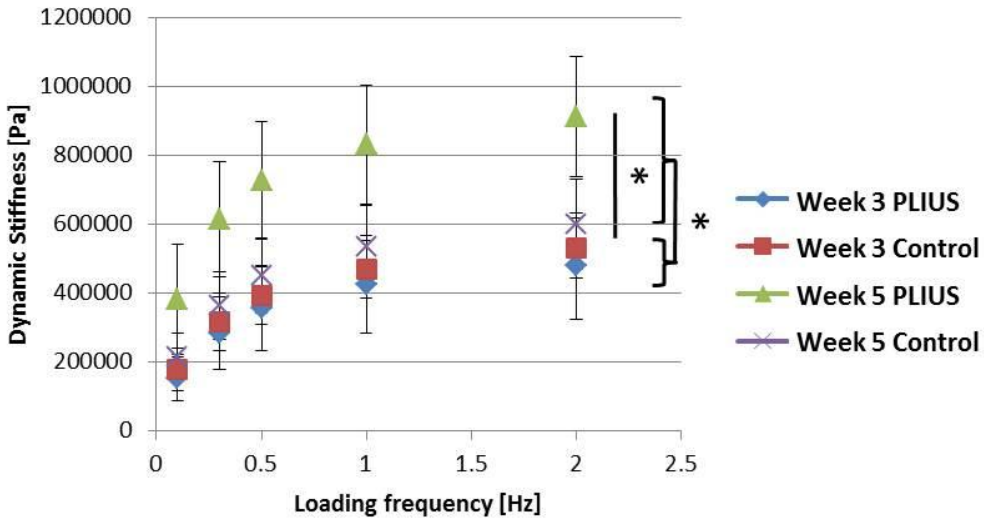

Figure 14. Dynamic stiffness over time with respect to treatment. (* $p < 0.05$)

found in this study after 5 weeks [46]. Though biochemical data is not reported for this study, collagen content was found by Hu et al. to increase exponentially over a 12-week timespan, with the bulk of the collagen deposition occurring after 6-8 weeks of culture [50]. If the length of time in culture for future experiments is increased to 12 weeks, the increase in collagenous matrix deposition may lead to further improved mechanical properties.

The mode of action on cells by PLIUS is not fully understood. Ultrasound has been shown to have two general modes of action which may affect cells in aqueous media: heating and micromechanical stimulation. However, pulsed ultrasound waves at intensity as low as the intended output of the transducers used here (30 mW/cm^2) have been shown to have negligible thermal effects on biological tissue [19, 27]. Therefore, the stimulation appears to be mechanical in nature. Pulsed ultrasound waves produce cavitation by oscillating gas microbubbles in aqueous media; this cavitation may be transient or stable [51]. Transient cavitation occurs when microbubbles oscillate asymmetrically and collapse on themselves, releasing the energy in extreme micro-

pockets of heat and pressure capable of causing cell lysis and necrosis [51]. However, work by Carstensen et al. showed that the intensity threshold for transient cavitation for microsecond-scale pulses was between 1 and 10 W/cm^2, two to three orders of magnitude greater than that used here [52]. As a result, adverse effects leading to cell damage have not been reported with the parameters used in this study [51]. Stable cavitation, by comparison, occurs when gas microbubbles oscillate without collapsing, producing ultrasonic waves radiating out from the bubble. Stable cavitation can lead to microstreaming, an effect whereby the ultrasonic waves around the cavitation bubbles cause standing micro-eddies which can vibrate cell membranes and may directly stimulate mechanoreceptors on cell surfaces [53]. As PLIUS was originally studied in bone fracture healing, its effect on fracture callus formation was studied extensively; the results conclusively show that PLIUS has an effect in improving callus formation and healing, but are inconclusive regarding the exact mechanism of action. Parvizi et al. reported findings that inhibition of calcium signaling inhibited the aggrecan upregulation and proteoglycan synthesis commonly associated with PLIUS [54]. In addition, a number of groups have recently attempted to answer the question by tracking signal pathway activation. Fitzgerald et al. subjected cartilage explants to static compression for 8 hours, finding that aggrecan and collagen II mRNA was temporarily upregulated, followed by catabolic factors MMP3, MMP9, and MMP13 being upregulated 24 hours later, leading to a net matrix degradation effect [55]. Meanwhile, work by De Croos et al. found that under a traditional cyclic loading regime, cartilage explants showed an initial burst of MMP 3 and MMP13 at 2 hours after loading, followed by upregulation of aggrecan and collagen II synthesis several hours later [24]. The work by De Croos et al. also showed

upregulation in genes associated with the MAPK signaling pathway, associated with matrix turnover. These results seem to imply that while static loading can cause matrix breakdown, cyclic loading may cause matrix to be broken down and replaced naturally. Recent work by Ito and colleagues with PLIUS showed a decrease in mRNA expression for MMP1 and MMP13 in both cartilage explants and rat chondrocyte monolayer cultures as soon as 1 hour after PLIUS treatment [56]. However, Takeuchi et al. cultured porcine chondrocytes on a collagen sponge scaffold with PLIUS treatment and found that the PI3K pathway (associated with cell proliferation) was preferentially activated over the MAPK pathway, and that collagen type IX (a regulatory collagen type believed to be associated with chondrocyte proliferation and attachment) was upregulated, while collagen type II was not [26]. It would seem by these results that traditional oscillatory cyclic loading and PLIUS act along two separate signaling pathways, but regulation of catabolic factor MMPs is similar in both, and Perry et al. showed that cyclic loading and PLIUS stimulation were not additive, implying that they actually do act on the same receptors [23]. The results of our study would seem to support the argument of De Croos (upregulation of matrix turnover), due to the increase in equilibrium and dynamic stiffnesses in the ultrasound-treated group from 3 to 5 weeks, implying greater net matrix deposition, but future work should elaborate upon this hypothesis.

The ultrasound parameters used here are used most often in PLIUS studies, but there is a significant spread regarding them, the physical setup of PLIUS stimulation, specimens, etc. The loading paradigm used in this study uses the FDA-approved parameters of 30 mW/cm^2 transducer intensity, 1.5 MHz oscillations at a burst rate of 1 kHz and duty cycle of 20% (i.e. 200 μs pulse of 1.5 MHz oscillation, 800 μs rest) for 20

minutes per day. There has been significant debate over what parameters produce the best results *in vitro*. For example, Zhang et al. showed that a reduction in intensity from 30 to 2 mW/cm^2 actually caused upregulation of collagen type II production in chick sternal chondrocytes encapsulated in alginate beads [57]. However, Ito and colleagues treated rat chondrocytes with PLIUS intensities of 0, 7.5, 30, and 120 mW/cm^2 and found a dose-dependent decrease in MMP13 production as the intensities increased [56]. Interestingly, the only intensity with which they showed significant mRNA upregulation of TIMP1 (an inhibitor of metalloproteinases) was 30 mW/cm^2. Irrechukwu et al. used an identical setup and treatment protocol to that used in our study, finding increases in proteoglycan and collagen type II synthesis and decreases in collagen type X (associated with cartilage degradation cascades) and MMP13, but this stands in opposition of Takeuchi et al. who also used an identical device and treatment protocol and showed no increase in collagen type II synthesis but increases in collagen type IX, a matrix protein associated with chondrocyte adhesion [26, 31]. A brief summary of several major tissue engineered cartilage studies using PLIUS is given in Table 1.

There were several points of this study which should be improved in future experiments building on this work. For example, larger sample sizes may lead to more statistically significant results. In addition, there are a number of other stimulation methods aside from PLIUS commonly used in tissue engineering. Growth factors, for example, have a substantial literature associated with them, and growth factor families such as bone morphogenic proteins and transcription growth factors have been described as having substantial benefit for growing cartilage [58-60]. While this study focused on delineating and quantifying the effects of PLIUS on tissue engineered cartilage,

interactions between the mechanical stimulation of PLIUS and biochemical stimulation of growth factors may strongly enhance both effects. Finally, while mechanical outcomes were deemed most important in this study, it did not take into account potential changes in composition associated with PLIUS, which biochemical assays may be able to identify. Future work should take into account each of these points.

Table 1. Summary of recent tissue-engineered cartilage studies performed using PLIUS stimulation

Group	Year	Cell source	Scaffold material	Ultrasound stimulation parameters	Ultrasound setup	Results
Irrechukwu et al.	2011	Bovine articular chondrocytes	Collagen gels	30 mW/cm^2, 1.5 MHz, 1 kHz burst rate, 20% duty cycle, 20 min/day	Transducers gel-coupled underneath well plates	↑ proteoglycan & collagen II, ↓ collagen X & MMP13
Baykal et al.	2010	Bovine articular chondrocytes	Collagen gels	30 mW/cm^2, 1.5 MHz, 1 kHz burst rate, 20% duty cycle, 20 min/day	Transducers gel-coupled underneath well plates	Near-IR spectral analysis
Bohari et al.	2012	NIH3T3 mouse fibroblasts	Alginate gels	200 mW/cm^2, 1 MHz, 20 Hz burst rate, 20% duty cycle, 5 min/day	Transducer immersed in water, well plate set on top	↑ proteoglycan & collagen, no added cell proliferation
Zhang et al.	2003	Chick intercostal cartilage chondrocytes	Alginate gels	30 or 2 mW/cm^2, 1.5 MHz, 1 kHz burst rate, 20% duty cycle, 20 min	Transducers gel-coupled to Parafilm floating on culture media in wells	↑cell proliferation, ↑ collagen II for 2 mW/cm^2 intensity, ↓collagen X
Takeuchi et al.	2008	Porcine articular chondrocytes	Collagen I sponges	30 mW/cm^2, 1.5 MHz, 1 kHz burst rate, 20% duty cycle, 20 min/day	Transducers gel-coupled to silicon rubber pad underneath well plates	↑collagen IX, no added collagen II, PI3K (matrix turnover) pathway upregulated
Choi et al.	2006	Human articular chondrocytes	Alginate gels	100, 200, or 300 mW/cm^2 standing wave, 1 MHz, 10 min/day	Transducers gel-coupled underneath well plates	↑ proteoglycan & collagen II, ↓ MMP1
Ito et al.	2012	Rat chondrocytes	Monolayer culture	7.5, 30, or 120 mW/cm^2, 1.5 MHz, 1 kHz burst rate, 20% duty cycle, 20 min/day	Transducers gel-coupled underneath well plates	↓ MMP13 was dose-dependent, ↑ TIMP1 at 30 mW/cm^2 only
Vaughan et al.	2010	Bovine articular chondrocytes	Alginate gels	30, 100, 200, or 300 mW/cm^2, 1.5 MHz, 1 kHz burst rate, 20% duty cycle, 20 min/day	Transducers gel-coupled underneath well plates	No change in cell proliferation for lower intensities, cell death in higher intensities; no progeoglycan changes at all

CHAPTER 4

SPECTROSCOPIC EVALUATION OF ENGINEERED CARTILAGE

Methods and Results: FT-IR Spectroscopic Evaluation of Crosslinks

To determine whether the 1660/1690 cm^{-1} collagen maturity ratio would be a useful parameter to study in cartilage, preliminary FT-IR tests were performed with purified pyridinoline crosslink peptides. Crosslink purification and data collection was performed by collaborators from the Yamauchi lab at the University of North Carolina (Chapel Hill, NC). Bovine articular cartilage was harvested from femoral condyles of a knee 4 h after slaughter in an FDA-approved slaughterhouse (JBS Souderton, Souderton, PA). Three age groups were used: fetal, young (2-3 weeks old) and mature (2-3 months old). Purified pyridinoline was separated from the cartilage via high-performance liquid chromatography (HPLC), deposited between two transmissive BaF_2 windows, and infrared spectra collected at 8 cm^{-1} spectral resolution and 25 μm spatial resolution in the mid-infrared range of 4000-760 cm^{-1} with 2 co-added scans per pixel, using a Perkin-Elmer Spectrum Spotlight 400 FT-IR imaging system (Perkin-Elmer, Shelton, CT) [42, 61-63].

The resultant spectra were averaged using ISys 5.0 spectral analysis software (Malvern Instruments, Malvern, UK). The spectra were baselined across the amide I band and the 1660/1690 cm^{-1} peak height ratio computed. The results are shown in Fig. 15. The spectral second derivative for each sample was computed using the Savitzky-Golay algorithm with an order of 3 and a window range of 7 cm^{-1} to show the presence of sub-band peaks at 1660 and 1690 cm^{-1}, and are shown in Fig. 16c. The amide I region of the spectra look distinctly different with increasing specimen age; this should not be the case if the 1660 and 1690 sub-band peaks directly correlate with crosslink peptides, and if the peptides are all the same and only differ in age of their tissue of origin.

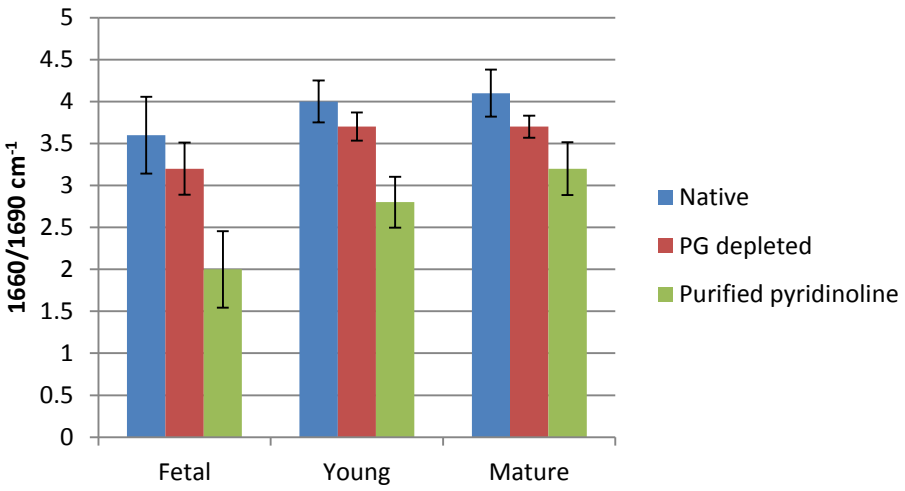

Figure 15. 1660/1690 cm-1 collagen maturity parameter for native cartilage, enzymatically proteoglycan-depleted cartilage, and pyridinoline peptide samples isolated from cartilage, taken from fetal, young (2-3 weeks old), and mature (2-3 months old) bovine specimens. Error bars show standard deviation across each sample.

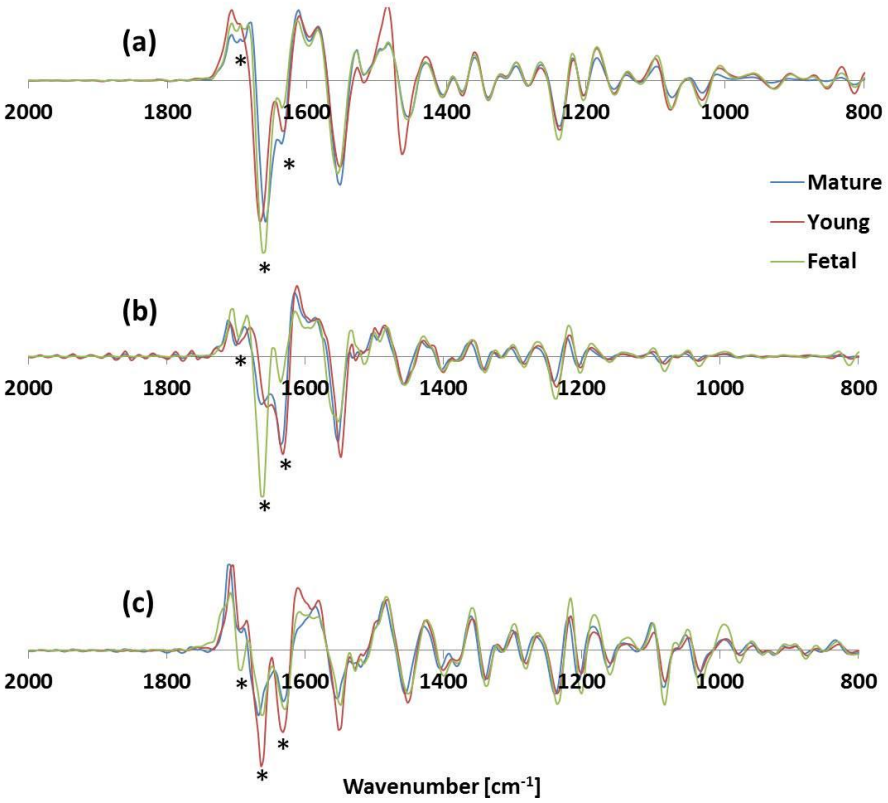

Figure 16. Second derivative spectra taken from (a) native cartilage, (b) enzymatically proteoglycan-depleted cartilage, and (c) pyridinoline crosslink peptides isolated from cartilage. Asterisks mark bands at 1630, 1660, and 1690 cm^{-1}. (Note that in second derivative spectra, relevant peaks are negative)

For comparison, second derivatives of native cartilage from the same three age groups were computed in the same manner, and are shown in Fig. 16a. The 1660/1690 cm^{-1} ratio for the three cartilage samples are shown in Fig. 15. Because proteoglycans do provide a small contribution to the amide I band in cartilage spectra, samples of cartilage from the three age groups were enzymatically degraded with hyaluronidase to selectively remove proteoglycans, leaving the collagen matrix intact. Sections were imaged and processed as above, and the second derivative spectra are shown in Fig. 16b and their 1660/1690 cm^{-1} ratios displayed alongside the others in Fig. 15. Second derivative spectra from before (native) and after proteoglycan depletion are compared in Fig. 17 for the three specimen age groups.

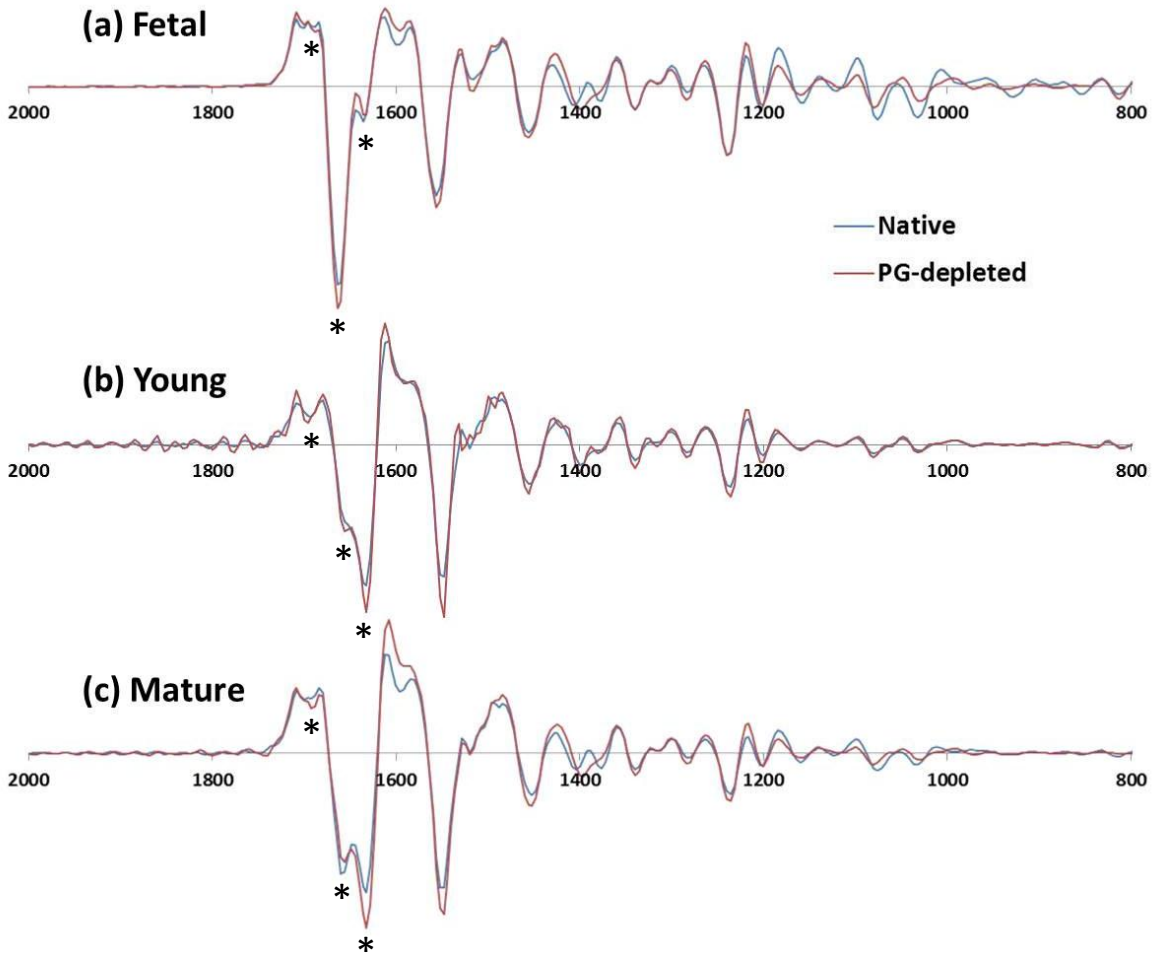

Figure 17. Second derivative spectra of cartilage samples before (native) and after hyaluronidase proteoglycan depletion over the three age groups.

Fig. 17 shows some curious points. Pure aggrecan (a common proteoglycan) is reported in literature to provide a contribution to the amide I band at 1640 cm^{-1}, and collagen/aggrecan spectral models have shown that increasing the proportion of aggrecan to collagen leads to an amide I shift from 1660 to lower frequencies, approaching 1640 [41]. Therefore, proteoglycan depletion should shift the amide I peak to a higher frequency, and should lead to decreased second derivative peaks at the lower-frequency end of the amide I region. However, this is only the case in the fetal specimen; the 1660 peak increases while the 1630 peak decreases with proteoglycan depletion. The young specimen shows decreases in both 1630 and 1660 peaks, with no discernible shift towards lower frequencies, and the mature specimen shows increases in the lower-frequency peak with proteoglycan depletion. If this method is adopted in future studies, this issue should be resolved prior to experimentation.

Based on the changes in 1660/1690 cm^{-1} ratio and second derivative spectral features observed across all sample groups with respect to age, it was determined that while this parameter does not appear to correlate quantitatively with different collagen crosslink types in a sample, it did increase with cartilage age and therefore may be a valuable measure of collagen "maturity." Because of this it was decided that it should be monitored over time and with respect to ultrasound stimulation, to assess whether there was correlation with mechanical or other parameters.

Methods: FT-IR Construct Analysis

Tissue engineered cartilage constructs from Aim 1 were analyzed spectroscopically. Constructs were halved down the center axis, formalin fixed, dehydrated, paraffin embedded, and histologically sectioned into 7 μm thick sections onto MirrIR low-emissivity microscope slides (Kevley Technologies, Chesterland, OH) which have no absorbance regions across the mid-infrared range. Sections were imaged using the aforementioned Perkin-Elmer Spectrum

Spotlight 400 FT-IR imaging system in transflectance mode over the mid-infrared range of 4000-760 cm^{-1} at 8 cm^{-1} spectral resolution and 25 μm spatial resolution and 2 co-added scans per pixel. Several parameters were then computed. Amide II (AM2), 1338 cm^{-1} (collagen side chain rotation, associated with collagen structural integrity), proteoglycan (850 cm^{-1}), and PGA (1750 cm^{-1}) peak areas were integrated, providing distribution maps of collagen, proteoglycans, and remaining scaffold material. Spectra were baselined and the ratio of peak height at 1660/1690 cm-1 computed as a measure of collagen crosslink/maturity. The ratio of 1338/AM2 peak areas was computed as a measure of collagen helical integrity [40, 41].

The images were then masked to only consider spectra from regions of higher collagen content. The second derivative was computed, and the collagenous regions were chosen by using the peak height of the 1338 cm^{-1} second derivative band. The 1338-masked regions were then analyzed for 1660/1690 ratio, 1338/AM2 ratio, and proteoglycan peak area.

Methods: Histological and Immunohistochemical Analyses

Sections were taken and stained histologically with Alcian blue for proteoglycans and hematoxylin/eosin for cell nuclei and background staining. To determine whether the chondrocytes seeded onto the scaffolds produced type I collagen, sections were also taken and stained via secondary antibody immunohistochemistry for collagen type I. Sections were deparaffinized and rehydrated, then washed 2x10 min with PBS buffer. Because proteoglycans take up so much space in cartilage, sections were treated with hyaluronidase solution (4800 U/mL in 0.025 M NaCl and 0.05 M sodium acetate in distilled water) for 2 hours at room temperature as a means of antigen retrieval, to reveal more collagen fibers for staining. Nonspecific binding was blocked through incubation with 5% BSA in PBS for 30 min at room temperature. Primary mouse monoclonal anti-bovine collagen type I antibodies were diluted 1:200 in 5% BSA/PBS and 50 μL drops were used to cover each section during incubation at

room temperature overnight. Samples were washed 2x10 min in PBS, then AlexaFluor 594-tagged donkey anti-mouse secondary antibodies were diluted to 1:600 and 50 μL drops used to cover the samples during 30 min incubation at room temperature. Samples were washed in PBS and incubated with 1:1000 DAPI stain for cell nuclei for 20 min at room temperature. After a final wash cycle, cover slips were mounted with Vectashield mounting medium and sealed with a clear acrylic coat.

Methods: Statistical Analysis

The spectroscopic data were explored through two-way ANOVA to determine the effects of time in culture and ultrasound treatment on the FTIR parameters, with Holm-Sidak post-hoc testing. In addition, Pearson correlations were assessed, with Pearson correlation coefficients (PCC) and p values reported to determine significance of positive and negative correlations between parameters at the $p < 0.05$ level. Finally, multiple linear regression (MLR) was used to create prediction models for mechanical data based on spectroscopic and geometric data.

Results

The results of the spectroscopic parameters discussed here are shown in Fig. 18. There was a significant decrease in PGA content over time. This is a logical result of PGA degradation throughout time in culture. Fig. 19 shows PGA distribution in a 3-week and 5-week specimen; visually, there is distinctly lower PGA absorbance after 5 weeks. There was no statistically significant difference in PGA area with respect to ultrasound treatment.

In addition the whole-construct 1338/AM2 collagen integrity parameter showed significantly higher collagen integrity in the ultrasound-treated group overall than in controls. Within the 5-week timepoint it was significantly higher in the ultrasound group, but no significant increase was seen at the 3-week timepoint. Interestingly, the measure of

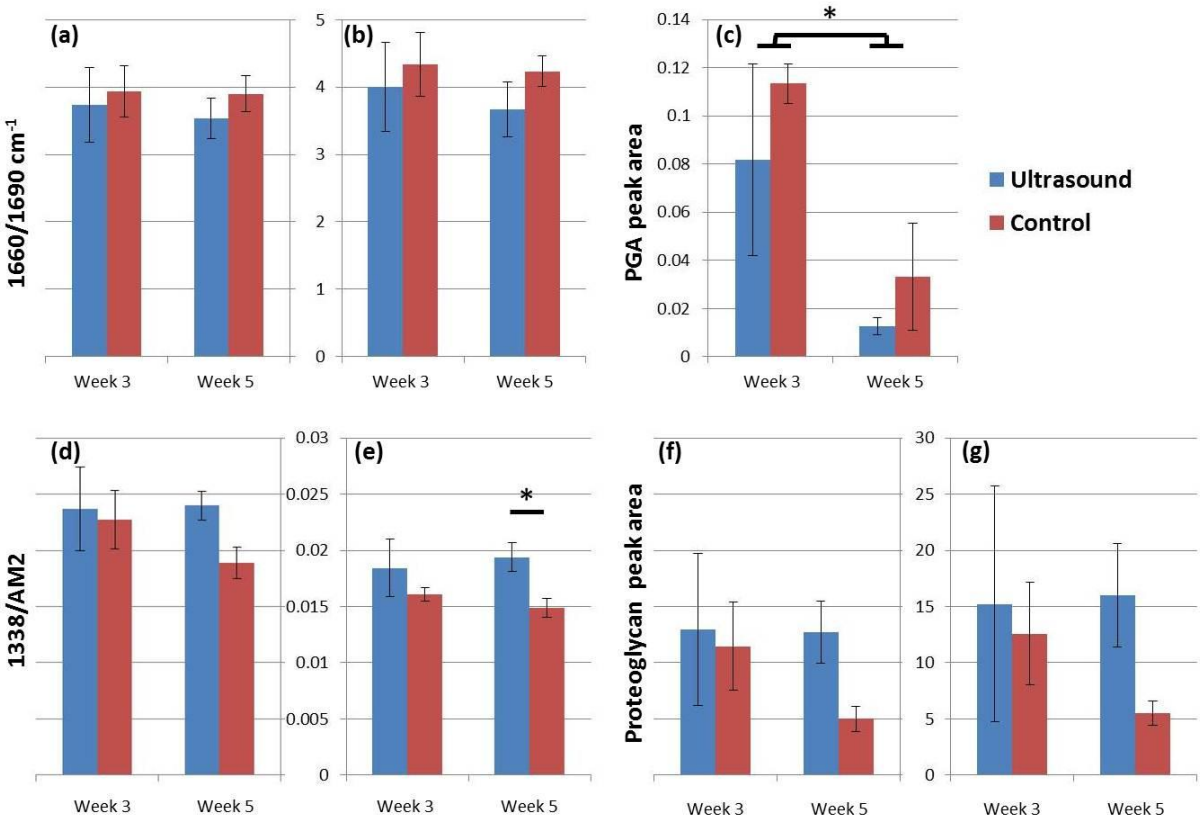

Figure 18. Spectroscopic and geometrical parameters measured from tissue engineered cartilage constructs. (a), (d), and (f) show parameters taken only from 1338-masked areas, while (b), (e), and (g) show parameters across entire construct. PGA content decreases significantly with time, and 1338/AM2 is significantly higher at 5 weeks in ultrasound-treated over control. (* $p < 0.05$)

1338/AM2 in just the high-collagen regions showed no commensurate significant increases. There were no significant changes revealed by ANOVA of the 1660/1690 cm^{-1} parameter or proteoglycan peak area (across the entire constructs or just in the high-collagen regions).

A correlation matrix based on the Pearson correlation analysis is presented in Table 2. Several interesting points may be made from this data. First, almost all of the spectral data correlated strongly with each other, either with positive or negative Pearson correlation coefficients (PCC). Proteoglycan peak area and the 1338/AM2 collagen integrity parameter

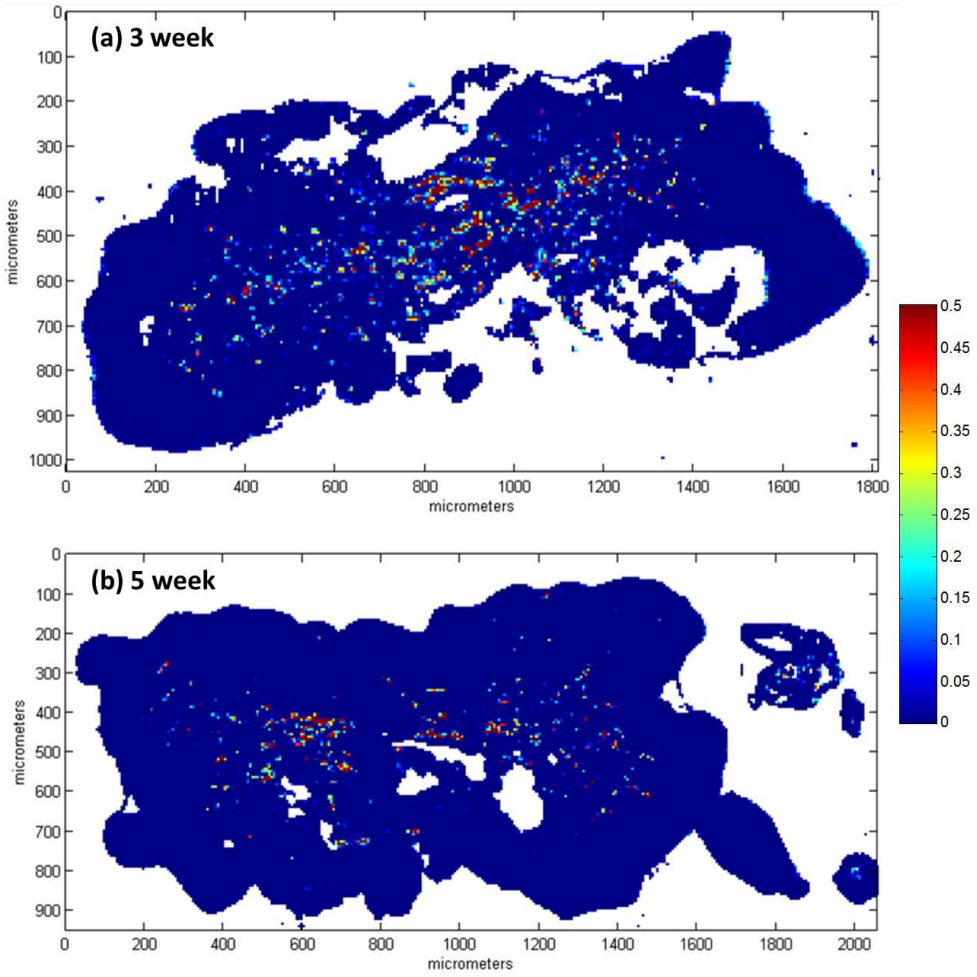

Figure 19. Maps of PGA distribution in representative constructs at (a) 3 weeks and (b) 5 weeks, based on the 1750 cm^{-1} peak area. The color bar represents the area under the PGA absorbance peak at 1750 cm^{-1}.

correlated inversely with the 1660/1690 cm^{-1} collagen maturity parameter (PCC = -0.838 and -0.661, respectively) The PGA peak area was found to correlate negatively to total geometrical cross-sectional area; while this may logically be attributed to the growth of the constructs and breakdown of the scaffold over time, geometrical area showed no statistically significant increase over time with two-way ANOVA. In addition, equilibrium stiffness and dynamic stiffness measured across all loading frequencies showed the expected strong positive

Table 2. Pearson correlation matrix of spectroscopic, mechanical and geometric data

	PG area	1338-masked 1338/AM2	1338/AM2	1338-masked 1660/1690	1660/1690	PGA area	Wet weight	Thickness	Area	Volume	Equilibrium Stiffness	Dynamic Stiffness
1338-masked PG area	0.977 5.22E-08	0.951 0.00000198	0.755 0.00455	-0.749 0.0051	-0.748 0.00516	-0.0261 0.936	0.0743 0.818	0.417 0.177	-0.426 0.168	-0.158 0.624	-0.00515 0.987	-0.0531 0.87
PG area		0.931 0.0000112	0.792 0.00216	-0.838 0.000663	-0.838 0.000672	-0.169 0.599	0.0794 0.806	0.275 0.387	-0.267 0.402	-0.096 0.767	0.0141 0.965	0.0365 0.91
1338-masked 1338/AM2			0.79 0.00221	-0.674 0.0162	-0.69 0.0131	-0.0908 0.779	-0.059 0.855	0.37 0.236	-0.352 0.261	-0.105 0.745	-0.0138 0.966	-0.0457 0.888
1338/AM2				-0.57 0.0528	-0.661 0.0194	-0.388 0.213	0.368 0.239	0.247 0.44	-0.168 0.603	0.0189 0.954	0.286 0.368	0.255 0.425
1338-masked 1660/1690					0.967 2.93E-07	0.47 0.123	-0.185 0.565	0.121 0.709	-0.104 0.748	-0.00477 0.988	-0.102 0.752	-0.211 0.509
1660/1690						0.572 0.0519	-0.267 0.402	0.0325 0.92	-0.0595 0.854	-0.0209 0.949	-0.22 0.493	-0.323 0.306
PGA area							-0.422 0.172	0.302 0.341	-0.614 0.0336	-0.471 0.122	-0.422 0.172	-0.498 0.0998
Wet weight								0.184 0.567	0.0232 0.943	0.21 0.513	0.37 0.236	0.225 0.482
Thickness									-0.568 0.0538	0.173 0.591	-0.0414 0.898	-0.231 0.469
Area										0.709 0.0099	0.0227 0.944	0.319 0.312
Volume											-0.0325 0.92	0.148 0.647
Equilibrium Stiffness												0.828 0.000873

Note: In each spot, top number is Pearson correlation coefficient and bottom is p value. Correlation coefficients are colored blue or red for positive or negative values, and darker colors represent higher values. Statistical significance denoted by p values highlighted in yellow ($p < 0.05$). Only dynamic stiffness measured at 2 Hz is shown, though all follow the same trend.

correlation. However, aside from the PGA/area correlation, no spectral data correlated with mechanical data with any significant level of statistical merit.

Multiple linear regression (MLR) models were created to attempt to predict the mechanical testing data using spectral and geometrical parameters. Different combinations were used, and a select few shown in Table 3. R, R^2, p value, and standard error of prediction (SEP) were reported. Models were created for equilibrium and dynamic stiffnesses using all four geometrical parameters (wet weight at harvest, construct thickness, construct cross-sectional area, and construct volume), the three whole-construct spectral parameters based on matrix components (1660/1690 cm^{-1}, 1338/AM2, and proteoglycan peak area), and a mix of spectral components including the collagen-based parameters from just the collagen-heavy areas and whole-construct data for non-collagen-based parameters. Plots of predicted versus actual equilibrium and dynamic stiffness values are presented in Fig. 21. Altogether, MLR analysis did not result in any models significant and robust enough to predict engineered cartilage mechanical properties from spectroscopic or geometrical data.

Discussion

The goal of this study was to assess the ability of FT-IR spectroscopy to identify and monitor changes in composition over time, and to correlate IR parameters (some well-validated, others not yet validated) with mechanical data.

The peak centered at 1338 cm^{-1} is specific to collagen in cartilage. In virtually all cases, the bulk of the 1338 peak distribution occurs around the very edges of the construct. A representative example of this may be seen in Fig. 22a. This is strongly indicative of a fibrous capsule created by the cells to surround the engineered cartilage construct. This hypothesis is supported by the immunohistochemical staining (Fig.20), which positively stained primarily the outer zone for collagen type I, indicative of fibrocartilage. Future work should stain for collagen

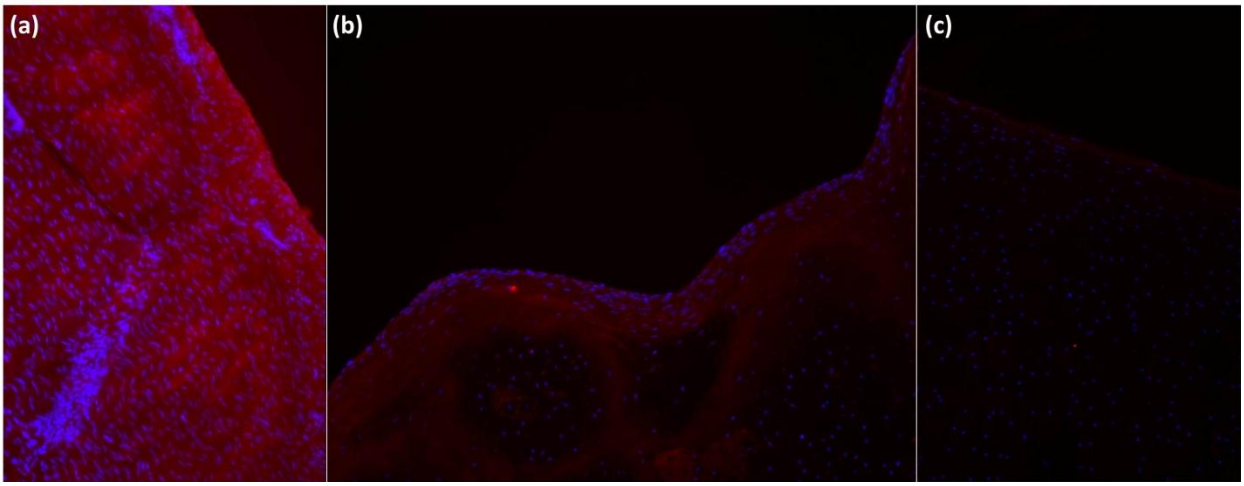

Figure 20. Immunohistochemical staining of collagen type I (red) and cell nuclei (DAPI, blue). (a) Bovine ACL cross-section (positive control). (b) 5 week ultrasound treated tissue engineered cartilage. (c) Bovine articular cartilage (negative control). Collagen type I is clearly positively stained in the superficial layer.

Table 3. Multiple linear regression results

Model from spectral data							
Equilibrium stiffness				**Dynamic stiffness (2 Hz)**			
Coefficient	**Variable**	**Statistics**		**Coefficient**	**Variable**	**Statistics**	
12206.711	Constant	R	0.448	1037841.99	Constant	R	0.518
-150669.247	PGA peak area	R^2	0.200	13809.786	PGA peak area	R^2	0.268
12925.584	1338-masked 1660/1690	p	0.778	-30372421.95	1338-masked 1338/AM2	p	0.650
-972352.686	1338-masked 1338/AM2	SEP	14229	64417.608	1338-masked 1660/1690	SEP	228276
844.556	Proteoglycan peak area			2388722.581	Proteoglycan peak area		
Model from spectral data, whole-construct matrix parameters only							
Equilibrium stiffness				**Dynamic stiffness (2 Hz)**			
Coefficient	**Variable**	**Statistics**		**Coefficient**	**Variable**	**Statistics**	
72498.138	Constant	R	0.591	1921129.264	Constant	R	0.653
-18597.505	1660/1690	R^2	0.349	-437034.85	1660/1690	R^2	0.427
4087922.876	1338/AM2	p	0.304	56554589.76	1338/AM2	p	0.195
-2161.461	PG peak area	SEP	12006	-39721.047	PG peak area	SEP	188931
Model from geometric data							
Equilibrium stiffness				**Dynamic stiffness (2 Hz)**			
Coefficient	**Variable**	**Statistics**		**Coefficient**	**Variable**	**Statistics**	
-488040.232	Constant	R	0.554	-10347804.44	Constant	R	0.623
244757.981	Wet weight	R^2	0.307	3082861.603	Wet weight	R^2	0.388
121275576.3	Thickness	p	0.574	2484776070	Thickness	p	0.424
15668797413	Area	SEP	13244	3.33991E+11	Area	SEP	208797
3967.002	Volume			80417.026	Volume		

type II as well to determine whether the outer zone is primarily fibrocartilage in nature or has hyaline-like qualities as well.

Another parameter which supports the theory that the chondrocytes are indeed still differentiated is the presence of proteoglycans throughout the center of the scaffolds, as seen in Fig. 22c. Proteoglycans are only produced by chondrocytes, and not by the fibroblast-like cells which chondrocytes dedifferentiate into. This is evidence towards the point that the cells in the scaffolds are indeed still phenotypically chondrocytic in nature.

However, if future staining does not show large amounts of collagen type II, it is a strong sign that the chondrocytes originally seeded onto the scaffold may have dedifferentiated back into a fibroblast-like morphology. Chondrocytes dedifferentiate to a fibroblast-like phenotype under a number of conditions, including high seeding density, high confluence in monolayer cultures, improper substrate mechanics, and biochemical insult [64]. The cell seeding density of $2 \cdot 10^7$ cells per scaffold was chosen due to previous work in our lab in which under-seeded scaffolds degraded too quickly (unpublished), presumably due to increased exposure to hydrolysis. The high seeding density may be a factor, though at present with the current PGA mesh scaffold material it would be impractical to lower the density and determine if it affects matrix production. In addition, the substrate mechanics may play a role. When chondrocytes are seeded onto hard substrates they can be negatively impacted. The Young's modulus of PGA is 6-7 GPa, well above that of natural cell substrates [65]. Use of a different substrate with similar degradation characteristics and better material properties may be an avenue of future work.

Another issue to consider is buildup of waste. Chondrocytes in native cartilage *in vivo* obtain most of their nutrients through synovial fluid flow through the extracellular matrix during loading and unloading. The paradigm used here is a static culture, in which no perfusion is

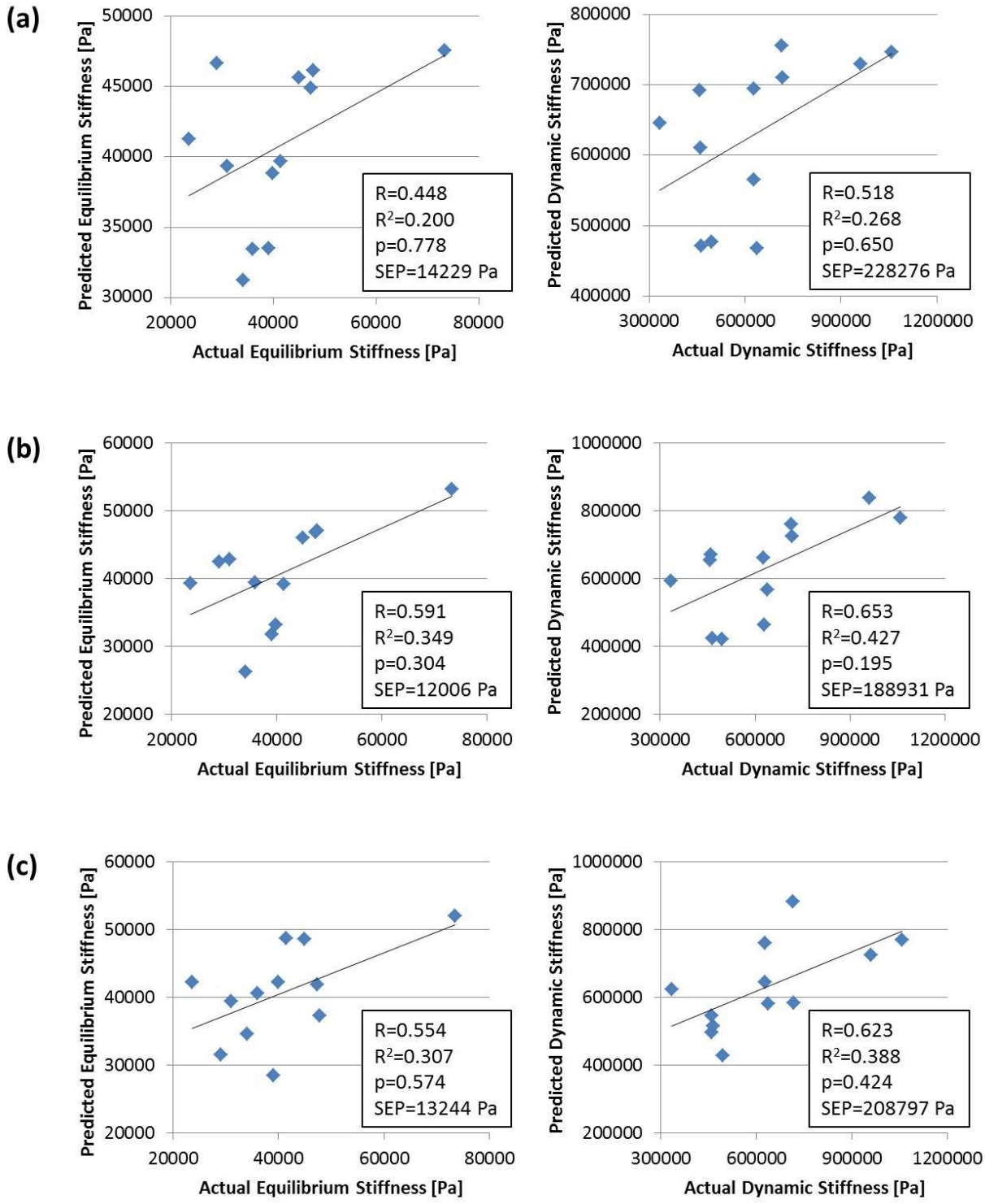

Figure 21. Multiple linear regression plots of actual vs. predicted values for mechanical testing data. (a) Model based on 1338-masked collagen based parameters (1660/1690, 1338/AM2) as well as proteoglycan and PGA distribution. (b) Model based on whole-construct spectral matrix parameters (1660/1690, 1338/AM2, proteoglycan). (c) Model based on geometric data (construct wet weight, thickness, area, volume).

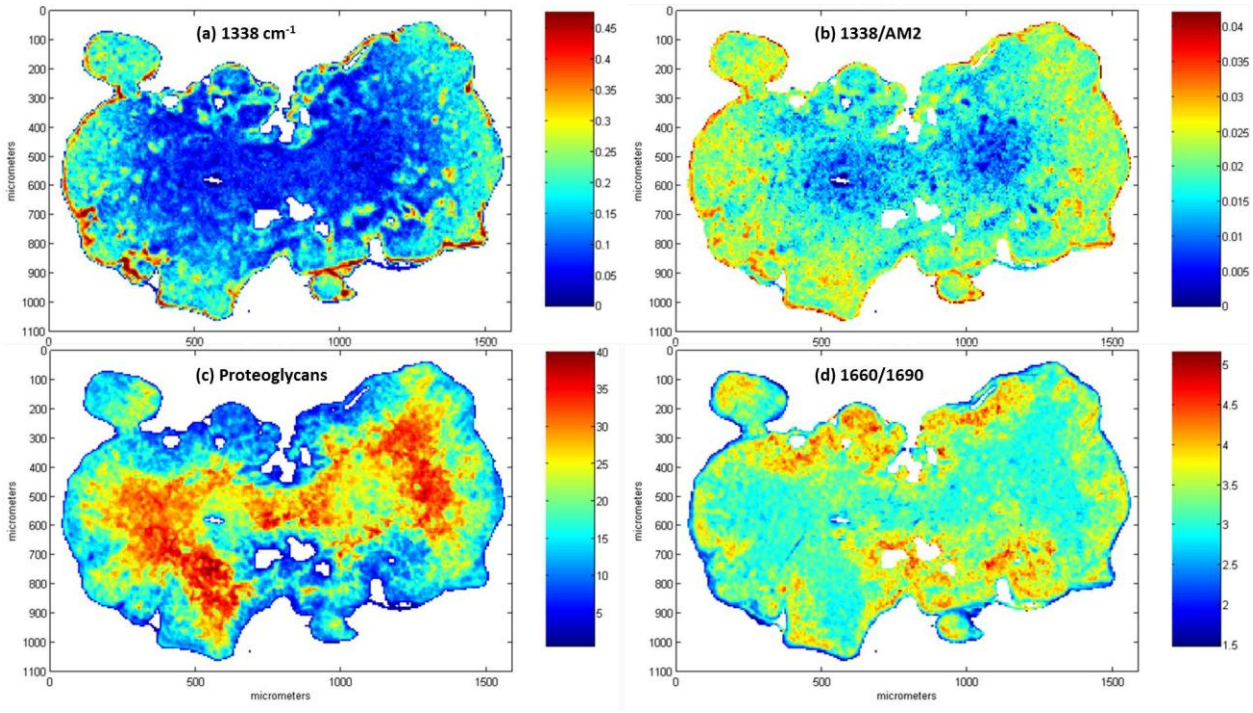

Figure 22. Compositional mapping of 5 week ultrasound treated cartilage construct, showing peak areas or ratios from spectra at each pixel. (a) 1338 cm^{-1} peak area distribution, (b) 1338/AM2 ratio, (c) proteoglycan peak area, (d) 1660/1690 cm^{-1} collagen maturity parameter. Color bars indicate area under absorbance peaks in (a) and (c), the ratio of peak areas in (b), and the ratio of peak heights at 1660 and 1690 cm^{-1} in (d).

present, relying primarily on diffusion through the matrix. This may prevent the cells from obtaining nutrients, and can lead to buildup of metabolic waste products and acidic waste products associated with PGA degradation. Perfusion flow bioreactors have been used to grow tissue engineered cartilage to some success by attachment of a peristaltic pump to create continuous media flow through the construct, not relying only on static diffusion for clearance of metabolic waste and scaffold breakdown products; this may be a means of improving chondrocyte health and therefore cartilage matrix production in future experiments [40, 46, 66, 67]. Another possibility could be the use of poly-L-lactic acid (PLLA) as a scaffold material; PLLA degrades into lactic acid monomers, found naturally in the body and resorbed readily. It degrades slower than PGA, over a matter of months, and may lead to less of a buildup of acidic

waste in the center of the constructs, where diffusion is the only clearance mechanism. Studies have shown that PLLA is not associated with the same acidity as PGA over a 12 hour period [68]. However, PGA was ultimately chosen because previous chondrocyte-based cell culture studies showed that over the first two months of culture, cell proliferation in PLLA scaffolds was half that of PGA scaffolds, but the same after six months [47]. This was presumably due to the lower degradation rate leading to space-restricted proliferation at first, until the PLLA scaffold had degraded sufficiently to allow full cell proliferation. As this study here had a total culture time of only 5 weeks, it was decided that the higher degradation rate of PGA would be beneficial.

The histology sections shown in Fig. 23 show distribution of cells, PGA fibers, and proteoglycan throughout the constructs. There is a superficial layer along the outer edge, which could be indicative either of the superficial zone of articular cartilage or the fibrous capsule formation mentioned earlier. In addition, there are several zones visible which seem to support the theory of waste buildup and diffusion issues. Fig. 24 is a histological section of a tissue engineered construct with several zones superimposed on it. There are three distinct regions: The superficial capsular layer, in which cells are morphologically arranged parallel to the surface; a middle zone which includes cells which appear healthy—larger, rounded, spread out, embedded in matrix, similar to the middle zone of native cartilage; and an inner region which is comprised of smaller cells at a much higher density, and which still includes PGA fibers (stained pink by eosin), and includes regions devoid of Alcian blue staining where cells have not produced much proteoglycan; the cells in this region show some perilacunar Alcian blue staining, but overall it is much less than the outer regions. This inner region is morphologically atypical of cartilage, and may be cells which have inadequate nutrient uptake and waste removal, and have reverted back

to a fibroblast-type morphology under the biochemical stresses imposed. Future work may include PCR or biochemical analyses to better elucidate this issue, and may benefit from serial sections taken for spectroscopic, histological and immunohistochemical assessment and direct correlation thereof.

The multiple linear regression models are shown in Table 3 and Fig. 21. The models based solely on geometrical data (wet weight, thickness, cross-sectional area, volume) may be used as a baseline for determining the effectiveness of models based on spectral data. Of the several listed here, the models with the lowest p value and SEP for both equilibrium and

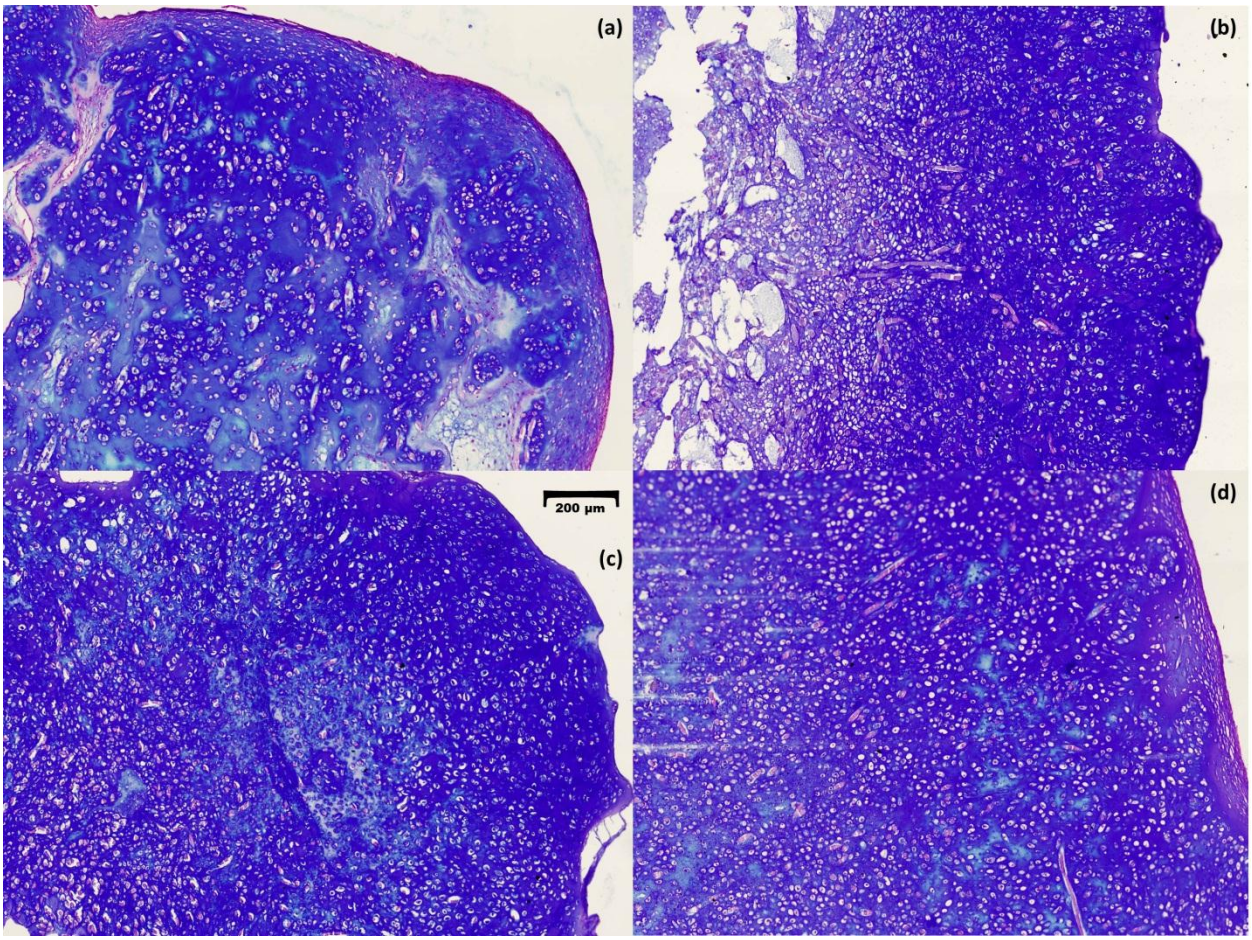

Figure 23. Histological staining of engineered cartilage constructs. Sections were stained with Alcian blue (proteoglycans) and hematoxylin & eosin (cell nuclei and background stain). (a) 3-week ultrasound treated, (b) 3-week control, (c) 5-week ultrasound treated, (d) 5-week control.

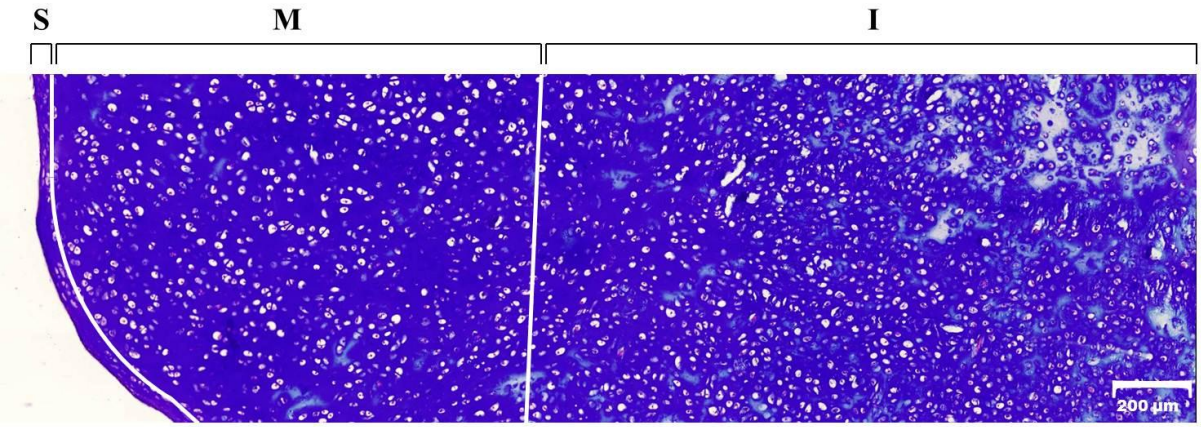

Figure 24. Histological staining of engineered cartilage construct with zonal boundaries superimposed. Visible are the superficial layer (S) containing elongated chondrocytes and slightly less Alcian blue staining (more pink), middle zone (M) showing heavy Alcian blue staining and lacunae visually similar to cartilage, and inner region (I) containing less Alcian blue staining and smaller, more densely packed cells.

dynamic stiffnesses were based on just three parameters: the 1660/1690 cm^{-1} collagen maturity parameter across the entire construct, the 1338/AM2 collagen integrity parameter across the entire construct, and the proteoglycan peak area. The relatively low number of variables leads to a more robust model than those which use more parameters to better fit the data. Despite the more logical choice of using the two collagen-based parameters only from the areas of high collagen, the models using these parameters performed poorly compared to others. This may be due to the fact that averaging across the entire construct may give a better indication of total collagen and its effect on the construct mechanical parameters. Future statistical analysis of spectral parameters may use multivariate analysis methods like principal component analysis to improve data investigation or partial least squares to obtain more useful prediction models.

The 1660/1690 cm^{-1} crosslink parameter has a significant body of literature associated with it when used in bone [40, 42, 43, 45]. However, its use in cartilage has not been studied at length. The amide I band is sensitive to protein secondary structure and is commonly used to

assess protein configurations [69]. As previously stated, the original publication introducing the 1660/1690 cm^{-1} parameter claimed a direct link to mature pyridinoline and immature DHLNL crosslinks, but since then the ratio has been regarded more as a measure of collagen maturity in the bone [43]. As an alternate hypothesis, it has been suggested that the parameter is a by-product of changes in the amide I peak due to changes in collagen secondary structure as bone matures and mineralizes around and through it [43]. This agrees in principle with recent work by Cui et al. showing conformational changes in collagen molecules during the biomineralization process [70]. Specifically, the group found that calcium binding to the collagen molecules occurred first, then phosphate groups bound the calcium ions into stable crystals; they proposed that this linkage system may lead to the collagen rotating about its axis to minimize interface energy as the calcium bound to it is pulled into place in the crystal lattice.

This is significantly different from the case of cartilage. In cartilage, the analogous space-filling, compression-resisting substance is proteoglycan and its associated water. Proteoglycans act in constant opposition to collagen, seeking to draw in more water and expand outwards, as collagen's superior tensile strength and crosslinked nature in turn acts to prevent this expansion in healthy cartilage. However, while proteoglycans do exert forces on the collagen matrix, they do not bond together as with the mineralization process in bone, so any associated conformational changes would be different in nature and therefore may manifest themselves differently in the FT-IR spectrum. The case for some conformational changes occurring over the aging process may be made with the preliminary experiments reported here, which found that the 1660/1690 ratio increased with increasing cartilage maturity in all specimens, but the sample size must be substantially inflated before those results may be considered meaningful. In particular, the sections of cartilage from which proteoglycans were removed still showed an increase in

1660/1690 ratio; however, this may be confounded by the formalin fixation of the samples prior to digestion, so that any conformational changes caused by proteoglycans may stay in the same conformation after the proteoglycans were removed. One possible method to rule out this situation could be to cryosection the samples rather than formalin fix and paraffin embed. Further study in this area is required before any conclusions may be drawn regarding the usefulness or uselessness of the 1660/1690 ratio.

One other possible avenue of future work may be to continue to pursue the use of HPLC. The ability to directly correlate spectral data with purified crosslinks could be a useful means of better understanding the 1660/1690 cm^{-1} collagen maturity parameter or possibly realizing another spectral feature which better correlates to specific crosslinks. To this end, it may be useful in future experiments to obtain crosslinks from tissue-engineered cartilage via HPLC separation for analysis and comparison to mechanical and spectral data.

CHAPTER 5

CONCLUSION

This work has explored the effects of pulsed low-intensity ultrasound on tissue engineered cartilage constructs, as well as methods of analysis thereof. A commercially available ultrasound transducer was assessed to confirm its output and effectiveness *in situ*, then shown to improve tissue engineered cartilage mechanically after 5 weeks in culture. These studies also investigated the basis for the PLIUS-related improved mechanical properties of cartilage. The primary findings were that although neither the FT-IR determined collagen content nor the collagen maturity parameter increased with PLIUS, the collagen integrity parameter, related to collagen maturation, did increase. In addition, FT-IR was able to detect and monitor PGA scaffold degradation over time. Thus, in summary, mechanical stimulation with PLIUS appears to improve mechanical properties in tissue engineered cartilage applications and may do so through improvement in collagen quality, but certainly additional studies are needed to validate these results.

REFERENCES

1. Fox, A.J.S., A. Bedi, and S.A. Rodeo, *The Basic Science of Articular Cartilage: Structure, Composition, and Function.* Sports Health: A Multidisciplinary Approach, 2009. **1**(6): p. 461-468.
2. Goldring, M.B. and S.R. Goldring, *Articular cartilage and subchondral bone in the pathogenesis of osteoarthritis.* Annals of the New York Academy of Sciences, 2010. **1192**(1): p. 230-237.
3. Mow, V.C., M.H. Holmes, and W. Michael Lai, *Fluid transport and mechanical properties of articular cartilage: a review.* Journal of biomechanics, 1984. **17**(5): p. 377-394.
4. Mow, V.C. and X.E. Guo, *Mechano-Electrochemical Properties of Articular Cartilage: Their Inhomogeneities and Anisotropies.* Annual Review of Biomedical Engineering, 2002. **4**(1): p. 175-209.
5. Park, S., et al., *Cartilage mechanical response under dynamic compression at physiological stress levels following collagenase digestion.* Annals of biomedical engineering, 2008. **36**(3): p. 425-434.
6. Korhonen, R.K., et al., *Comparison of the equilibrium response of articular cartilage in unconfined compression, confined compression and indentation.* Journal of biomechanics, 2002. **35**(7): p. 903-909.
7. Martin, I., et al., *Modulation of the mechanical properties of tissue engineered cartilage.* Biorheology, 2000. **37**(1): p. 141-147.
8. Park, S., C.T. Hung, and G.A. Ateshian, *Mechanical response of bovine articular cartilage under dynamic unconfined compression loading at physiological stress levels.* Osteoarthritis and Cartilage, 2004. **12**(1): p. 65-73.
9. Frank, E.H. and A.J. Grodzinsky, *Cartilage electromechanics: A continuum model of cartilage electrokinetics and correlation with experiments.* Journal of biomechanics, 1987. **20**(6): p. 629-639.
10. Frenkel, S.R., et al., *Regeneration of articular cartilage: Evaluation of osteochondral defect repair in the rabbit using multiphasic implants.* Osteoarthritis and Cartilage, 2005. **13**(9): p. 798-807.
11. Newman, A.P., *Articular cartilage repair.* The American journal of sports medicine, 1998. **26**(2): p. 309-324.
12. Safran, M.R. and K. Seiber, *The Evidence for Surgical Repair of Articular Cartilage in the Knee.* Journal of the American Academy of Orthopaedic Surgeons, 2010. **18**(5): p. 259-266.
13. Bentley, G., et al., *A prospective, randomised comparison of autologous chondrocyte implantation versus mosaicplasty for osteochondral defects in the knee.* Journal of Bone & Joint Surgery, British Volume, 2003. **85-B**(2): p. 223-230.
14. Temenoff, J.S. and A.G. Mikos, *Review: tissue engineering for regeneration of articular cartilage.* Biomaterials, 2000. **21**(5): p. 431-440.
15. Vunjak-Novakovic, G., et al., *Effects of mixing on the composition and morphology of tissue-engineered cartilage.* AIChE journal, 1996. **42**(3): p. 850-860.
16. Indian Institute of Technology Delhi, D.o.T.T. *Tissue Engineering.* 2013 [cited; Available from: http://textile.iitd.ac.in/highlights/fol8/01.htm.
17. Malizos, K.N., et al., *Low-intensity pulsed ultrasound for bone healing: an overview.* Injury, 2006. **37**(1): p. S56-S62.
18. Pounder, N.M. and A.J. Harrison, *Low intensity pulsed ultrasound for fracture healing: A review of the clinical evidence and the associated biological mechanism of action.* Ultrasonics, 2008. **48**(4): p. 330-338.
19. Weidman, J. and J. Tavakkoli, *Concurrent heat and ultrasound treatment does not im-prove mineralization in bone cell cultures in vitro.*
20. Cook, S.D., et al., *The Effect of Low-Intensity Pulsed Ultrasound on Autologous Osteochondral Plugs in a Canine Model.* The American journal of sports medicine, 2008. **36**(9): p. 1733-1741.

21. Gurkan, I., et al., *Modification of osteoarthritis in the guinea pig with pulsed low-intensity ultrasound treatment.* Osteoarthritis and Cartilage, 2010. **18**: p. 724-733.
22. Torzilli, P.A., M. Bhargava, and C.T. Chen, *Mechanical Loading of Articular Cartilage Reduces IL-1-Induced Enzyme Expression.* Cartilage, 2011. **2**(4): p. 364-373.
23. Perry, M.J., et al., *Ultrasound mimics the effect of mechanical loading on bone formation in vivo on rat ulnae.* Medical Engineering & Physics, 2009. **31**(1): p. 42-47.
24. De Croos, J.N.A., et al., *Cyclic compressive mechanical stimulation induces sequential catabolic and anabolic gene changes in chondrocytes resulting in increased extracellular matrix accumulation.* Matrix Biology, 2006. **25**(6): p. 323-331.
25. Fanning, P.J., et al., *Mechanical Regulation of Mitogen-activated Protein Kinase Signaling in Articular Cartilage.* Journal of Biological Chemistry, 2003. **278**(51): p. 50940-50948.
26. Takeuchi, R., et al., *Low-intensity pulsed ultrasound activates the phosphatidylinositol 3 kinase/Akt pathway and stimulates the growth of chondrocytes in three-dimensional cultures: a basic science study.* Arthritis Research and Therapy, 2008. **10**(4): p. 77.
27. Chang, W.H.S., et al., *Study of thermal effects of ultrasound stimulation on fracture healing.* Bioelectromagnetics, 2002. **23**(4): p. 256-263.
28. Loyola-Sánchez, A., et al., *Effect of Low-Intensity Pulsed Ultrasound on the Cartilage Repair in People With Mild to Moderate Knee Osteoarthritis: A Double-Blinded, Randomized, Placebo-Controlled Pilot Study.* Archives of physical medicine and rehabilitation, 2012. **93**(1): p. 35-42.
29. Bohari, S.P.M., L.M. Grover, and D.W.L. Hukins, *Pulsed-low intensity ultrasound enhances extracellular matrix production by fibroblasts encapsulated in alginate.* Journal of Tissue Engineering, 2012.
30. Choi, B.H., et al., *Low-intensity ultrasound stimulates the viability and matrix gene expression of human articular chondrocytes in alginate bead culture.* Journal of Biomedical Materials Research Part A, 2006. **79A**(4): p. 858-864.
31. Irrechukwu, O., et al., *Magnetic Resonance Studies of Macromolecular Content in Engineered Cartilage Treated with Pulsed Low-Intensity Ultrasound.* Tissue Engineering A, 2011. **17**(3-4): p. 407-415.
32. Eyre, D.R. and J.J. Wu, *Collagen cross-links.* Collagen, 2005: p. 207-229.
33. Robins, S.P. and J.D. Brady, *Collagen cross-linking and metabolism.* Principles of bone biology, 2002. **1**: p. 211-223.
34. Bailey, A.J., R.G. Paul, and L. Knott, *Mechanisms of maturation and ageing of collagen.* Mechanisms of ageing and development, 1998. **106**(1): p. 1-56.
35. Ahsan, T., et al., *Kinetics of collagen crosslinking in adult bovine articular cartilage.* Osteoarthritis and Cartilage, 2005. **13**(8): p. 709-715.
36. Turunen, M.J., et al., *Age-related changes in organization and content of the collagen matrix in rabbit cortical bone.* Journal of Orthopaedic Research, 2011. **30**(3): p. 435-442.
37. Williamson, A.K., et al., *Tensile mechanical properties of bovine articular cartilage: Variations with growth and relationships to collagen network components.* Journal of Orthopaedic Research, 2003. **21**(5): p. 872-880.
38. Bastiaansen-Jenniskens, Y.M., et al., *Contribution of collagen network features to functional properties of engineered cartilage.* Osteoarthritis and Cartilage, 2008. **16**(3): p. 359-366.
39. Eyre, D.R., M.A. Weis, and J.-J. Wu, *Advances in collagen cross-link analysis.* Methods, 2008. **45**: p. 65-74.
40. Boskey, A. and N. Pleshko Camacho, *FT-IR imaging of native and tissue-engineered bone and cartilage.* Biomaterials, 2007. **28**: p. 2465-2478.
41. Camacho, N.P., et al., *FTIR microscopic imaging of collagen and proteoglycan in bovine cartilage.* Biopolymers, 2001. **62**(1): p. 1-8.
42. Paschalis, E.P., et al., *Spectroscopic Characterization of Collagen Cross-Links in Bone.* Journal of bone and mineral research, 2001. **16**(10): p. 1821-1828.

43. Farlay, D., et al., *The ratio 1660/1690 cm− 1 measured by infrared microspectroscopy is not specific of enzymatic collagen cross-links in bone tissue.* PloS one, 2011. **6**(12): p. e28736.
44. Barth, H., *Characterization of the effects of x-ray irradiation on the hierarchical structure and mechanical properties of human cortical bone*. 2012, Lawrence Berkeley National Laboratory.
45. Ruppel, M.E., D.B. Burr, and L.M. Miller, *Chemical makeup of microdamaged bone differs from undamaged bone.* Bone, 2006. **39**(2): p. 318-324.
46. Vunjak-Novakovic, G., et al., *Bioreactor cultivation conditions modulate the composition and mechanical properties of tissue-engineered cartilage.* Journal of Orthopaedic Research, 1999. **17**(1): p. 130-138.
47. Freed, L.E., et al., *Neocartilage formation in vitro and in vivo using cells cultured on synthetic biodegradable polymers.* Journal of biomedical materials research, 1993. **27**(1): p. 11-23.
48. Pfeiffer, E., et al., *The effects of glycosaminoglycan content on the compressive modulus of cartilage engineered in type II collagen scaffolds.* Osteoarthritis and Cartilage, 2008. **16**(10): p. 1237-1244.
49. Frampton, R. *The Dynamic Testing of Elastomers*. Alpha Testing Systems Ltd 2013 [cited; Available from: http://www.alphatestingsystems.com/RFdynamic-testingPaper.pdf.
50. Hu, J.C. and K.A. Athanasiou, *A self-assembling process in articular cartilage tissue engineering.* Tissue Engineering, 2006. **12**(4): p. 969-979.
51. Maulik, D., *Biologic effects of ultrasound.* Clinical obstetrics and gynecology, 1989. **32**(4): p. 645-659.
52. Carstensen, E.L. and H.G. Flynn, *The potential for transient cavitation with microsecond pulses of ultrasound.* Ultrasound in medicine & biology, 1982. **8**(6): p. L720.
53. Wang, S.-J., et al., *Low intensity ultrasound treatment increases strength in a rat femoral fracture model.* Journal of Orthopaedic Research, 1994. **12**(1): p. 40-47.
54. Parvizi, J., et al., *Calcium signaling is required for ultrasound-stimulated aggrecan synthesis by rat chondrocytes.* Journal of Orthopaedic Research, 2002. **20**(1): p. 51-57.
55. Fitzgerald, J.B., et al., *Mechanical compression of cartilage explants induces multiple time-dependent gene expression patterns and involves intracellular calcium and cyclic AMP.* Journal of Biological Chemistry, 2004. **279**(19): p. 19502-19511.
56. Ito, A., et al., *Low-Intensity Pulsed Ultrasound Inhibits Messenger RNA Expression of Matrix Metalloproteinase-13 Induced by Interleukin-1 in Chondrocytes in an Intensity-Dependent Manner.* Ultrasound in medicine & biology, 2012. **38**(10): p. 1726-1733.
57. Zhang, Z.-J., et al., *The effects of pulsed low-intensity ultrasound on chondrocyte viability, proliferation, gene expression and matrix production.* Ultrasound in medicine & biology, 2003. **29**(11): p. 1645-1651.
58. Chubinskaya, S., M. Hurtig, and D.C. Rueger, *OP-1/BMP-7 in cartilage repair.* International orthopaedics, 2007. **31**(6): p. 773-781.
59. Fortier, L.A., et al., *The role of growth factors in cartilage repair.* Clinical Orthopaedics and Related ResearchÂ®, 2011. **469**(10): p. 2706-2715.
60. Hickey, D.G., S.R. Frenkel, and P.E. Di Cesare, *Clinical applications of growth factors for articular cartilage repair.* American journal of orthopedics (Belle Mead, NJ), 2003. **32**(2): p. 70.
61. Yamauchi, M., et al., *Structure and formation of a stable histidine-based trifunctional cross-link in skin collagen.* Journal of Biological Chemistry, 1987. **262**(24): p. 11428-11434.
62. Yamauchi, M. and M. Shiiba, *Lysine Hydroxylation and Cross-linking of Collagen: Post-translational Modifications of Proteins.* 2008. **446**: p. 95-108.
63. Yamauchi, M. and M. Shiiba, *Lysine hydroxylation and crosslinking of collagen*, in *Posttranslational Modifications of Proteins*. 2002, Springer. p. 277-290.
64. Schulze-Tanzil, G., *Activation and dedifferentiation of chondrocytes: implications in cartilage injury and repair.* Ann Anat, 2009. **191**(4): p. 325-38.
65. International, A.S.M., *Materials and Coatings for Medical Devices: Cardiovascular*. 2009: American Society for Microbiology.

66. Kim, M., et al. *Development and analysis of tissue-engineered mammalian cartilage in a hollow-fiber bioreactor: FTIR spectroscopic and gene expression studies*. in *6th Symposium of the International Cartilage Repair Society*. 2006.
67. Sailon, A.M., et al., *A Novel Flow-Perfusion Bioreactor Supports 3D Dynamic Cell Culture.* Journal of Biomedicine and Biotechnology, 2009. **2009**.
68. Sittinger, M., et al., *Resorbable polyesters in cartilage engineering: Affinity and biocompatibility of polymer fiber structures to chondrocytes.* Journal of biomedical materials research, 1996. **33**(2): p. 57-63.
69. Barth, A., *Infrared spectroscopy of proteins.* Biochimica et Biophysica Acta (BBA) - Bioenergetics, 2007. **1767**(9): p. 1073-1101.
70. Cui, F.Z., et al., *Conformation change of collagen during the initial stage of biomineralization of calcium phosphate.* Journal of Materials Chemistry, 2008. **18**(32): p. 3835-3840.